ARO 20576.3-GS

Report SDSMT/IAS/R-86/03   April 1986

A DETAILED ANALYSIS OF THE INFLUENCE OF EDDY
EXCHANGE PROCESSES UPON THE DEVELOPMENT OF
RADIATION FOG

By: Ronald M. Welch

Prepared for:

86 6   2

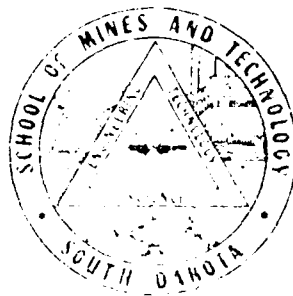| REPORT DOCUMENTATION PAGE		READ INSTRUCTIONS BEFORE COMPLETING FORM
1. REPORT NUMBER *ARO 205-76.3-GS*	2. GOVT ACCESSION NO. N/A	3. RECIPIENT'S CATALOG NUMBER N/A
4. TITLE *(and Subtitle)* A Detailed Analysis of the Influence of Eddy Exchange Processes Upon the Development of Radiation Fog		5. TYPE OF REPORT & PERIOD COVERED Final Technical Report 9/19/83-3/18/86
		6. PERFORMING ORG. REPORT NUMBER
7. AUTHOR(s) Ronald M. Welch		8. CONTRACT OR GRANT NUMBER(s) DAAG29-83-K-0165
9. PERFORMING ORGANIZATION NAME AND ADDRESS Institute of Atmospheric Sciences S.D. School of Mines and Technology Rapid City, SD 57701-3995		10. PROGRAM ELEMENT, PROJECT, TASK AREA & WORK UNIT NUMBERS
11. CONTROLLING OFFICE NAME AND ADDRESS U. S. Army Research Office Post Office Box 12211 Research Triangle Park, NC 27709		12. REPORT DATE April 1986
		13. NUMBER OF PAGES 8 + appendices
14. MONITORING AGENCY NAME & ADDRESS*(If different from Controlling Office)*		15. SECURITY CLASS. *(of this report)* Unclassified
		15a. DECLASSIFICATION/DOWNGRADING SCHEDULE

16. DISTRIBUTION STATEMENT *(of this Report)*

Approved for public release; distribution unlimited.

17. DISTRIBUTION STATEMENT *(of the abstract entered in Block 20, if different from Report)*

NA

18. SUPPLEMENTARY NOTES

The view, opinions, and/or findings contained in this report are those of the author(s) and should not be construed as an official Department of the Army position, policy, or decision, unless so designated by other documentation.

19. KEY WORDS *(Continue on reverse side if necessary and identify by block number)*

Fog, radiation, turbulence, exchange, Landsat, periodic oscillations

20. ABSTRACT *(Continue on reverse side if necessary and identify by block number)*

After decades of theoretical development, fog models have evolved to the point of qualitative agreement with observations. Current models are capable of simulating observed quasi-periodic oscillations in fog variables as well as the various stages of fog growth. It is now anticipated that continued efforts towards greater model sophistication will lead to at least limited quantitative agreement with observations and improved predictive capability.

CONTINUED

DD FORM 1 JAN 73 **1473** EDITION OF 1 NOV 65 IS OBSOLETE

20. Abstract (Continued)

Application of very high resolution Landsat digital data to fog episodes has revealed the stratocumulus nature of fog. That other satellite imagery has shown little hint of this cellular structure is due to the fact that the fog elements are generally smaller than the spatial resolution available on these satellite platforms. The ratio of wavelength between cells and the height of the boundary layer is in agreement with values obtained for Benard cells and longitudinal rolls in cloud systems. The processes occurring in fogs are similar, but on a smaller scale, to those responsible for these boundary layer cloud systems. Therefore, further studies of fog processes are expected to provide quantitative information concerning the processes responsible for Benard cells, longitudinal rolls and cloud top entrainment instability.

A DETAILED ANALYSIS OF THE INFLUENCE OF EDDY EXCHANGE
PROCESSES UPON THE DEVELOPMENT OF RADIATION FOG

FINAL TECHNICAL REPORT

RONALD M. WELCH

APRIL 1986

U. S. ARMY RESEARCH OFFICE

CONTRACT NO. DAAG29-83-K-0165

INSTITUTE OF ATMOSPHERIC SCIENCES
SOUTH DAKOTA SCHOOL OF MINES AND TECHNOLOGY
RAPID CITY, SOUTH DAKOTA   57701-3995

APPROVED FOR PUBLIC RELEASE;

DISTRIBUTION UNLIMITED.

FOREWARD

~After decades of theoretical development, fog models have evolved
to the point of qualitative agreement with observations. Current
models are capable of simulating observed quasi-periodic oscillations
in fog variables as well as the various stages of fog growth. It is
now anticipated that continued efforts towards greater model sophisti-
cation will lead to at least limited quantitative agreement with
observations and improved predictive capability.

Application of very high resolution Landsat digital data to fog
episodes has revealed the stratocumulus nature of fog. That other
satellite imagery has shown little hint of this cellular structure is
due to the fact that the fog elements are generally smaller than the
spatial resolution available on these satellite platforms. The ratio
of wavelength between cells and the height of the boundary layer is in
agreement with values obtained for Benard cells and longitudinal rolls
in cloud systems. The processes occurring in fogs are similar, but on
a smaller scale, to those responsible for these boundary layer cloud
systems. Therefore, further studies of fog processes are expected to
provide quantitative information concerning the processes responsible
for Benard cells, longitudinal rolls and cloud top entrainment
instability.

TABLE OF CONTENTS

LIST OF APPENDICES

1. STATEMENT OF PROBLEM

Fog is a mesoscale boundary layer phenomena which generally forms under high pressure and stable conditions after nocturnal cooling lowers the near-surface temperature to the dew point. However, the process of fog formation is in dispute. Observations in England by Roach et al. (1976) showed that fog forms only after wind speeds decrease to low values, so that turbulence is nearly non existent. On the other hand Rodhe (1962) suggested that fog formation is the reuslt of the turbulent mixing of nearly saturated eddies at different temperatures. Lala et al. (1982) found that freshening of calm winds, causing reduced stability and increased turbulence, contributes to fog formation.

Roach (1976) was the first to observe that fogs often have quasi-periodic oscillations of longwave radiation, surface temperature, visibility and wind speed. Gerber (1981) found that dense fog was composed of highly structured and sharply defined local regions. Other observations by Jiusto and Lala (1983) have identified five distinct stages of fog develoment and dissipation.

Fog prediction models also have grown in sophistication but, to date, no model has reproduced observations with any degree of satisfaction. Mutual interactions of turbulence, radiation and thermodynamics make fog simulations a very complicated problem. The choice of turbulence formulation appears to be the single most important factor determining fog development.

The purpose of the present study has been to develop improved models capable of simulating the qualitative behavior of radiation fogs. The observations of Jiusto and Lala at Albany, New York, have been used for initiation and verification. The investigation was directed towards comparison of predictions made with a whole range of increasingly more complicated turbulence modes. The goal was to identify the least complex model capable of producing reasonably accurate predictions.

2. SUMMARY OF RESULTS

Due to their inherent simplicity, and also due to the fact that such approaches are computationally less expensive than higher-order closure techniques, similarity-theory turbulence parameterizations have been widely used in the meteorology community. This was the approach taken in the present studies. It was surprising to see how well stability-corrected versions of similarity theory were able to produce fog profiles which were in qualitative agreement with the Jiusto and Lala observations.

Six different turbulent exchange formulations were applied, based either upon measurements or upon simplifications of second-order clo-

sure approximations. Three different Monin-Obukhov stability functions were specified, along with different parameterizations of Richardson number and mixing length. The subset of results presented in Appendix 1 shows the range of variability encountered by using these different formulations for turbulent mixing.

While there are some large differences between the results, the similarities are more important. Note that the various models simulate the five stages of fog development as observed by Jiusto and Lala. Second, the quasi-periodic behavior of the fog variables also is simulated. Considering the crudeness of the exchange parameterizations, the qualitative agreement with observations indeed is surprising. The results show that fog formation and development is directly correlated with the magnitude of the eddy mixing coefficients. Larger turbulence generation leads to more rapid fog development and to lower visibilities. During the mature fog stage a series of fog dissipation and redevelopment episodes occur. In the upper portion of the fog, radiative cooling causes development of large liquid water contents during turbulently quiet periods. Subsequent destabilization mixes the upper level liquid water to the surface, creating the observed periods of surface fog intensification. A thorough report of this behavior is found in Appendix 1.

The periodicity of 15-20 minutes observed in the various fog parameters is not reproduced in the simulations. Rather, depending upon the turbulence formulation, periodicities on the order of 40-60 minutes are predicted. However, the LANDSAT observations offer a possible explanation. Considering the typical size of fog cells, the fact that their typical horizontal aspect ratio is a value of two, and that typical wind speed in fogs is on the order of 2m/s, advection of fog cells across a fixed site would cause a variability in fog parameters of 16-18 min. Details are given in Appendix 2.

A number of investigators have studied the relationship of cloud element size and the height of the boundary layer. The ratio of wavelength to the height of the boundary layer in cloud systems is typically in the range of 2-6. For fogs we found values of 2-3. While the results are tentative due to the small number of cases studied, it is suggested that processes occurring in fogs are similar, but on a smaller scale, to those processes responsible for Benard cloud cells, longitudinal rolls, and cloud top entrainment instability. It is anticipated that improved understanding of fog processes will lead to corresponding improvement in our understanding of cloud processes.

3. LIST OF PUBLICATIONS

1. "Prediction of Quasi-Periodic Oscillations in Radiation Fogs. Part I: Comparison of Simple Similarity Approaches" by R. M. Welch, M. G. Ravichandran and S. K. Cox, 1986, J. Atmos. Sci., 43, _____.

2. "The Stratocumulus Nature of Fog" by R. M. Welch and B. A. Wielicki, 1986, J. Climate Appl. Meteor., 25, 101-111.

3. "Periodicity in Radiation Fog" by R. W. Welch and M. G. Ravichandran. IAMAP/IAPSO Joint Assembly, 5-16 August 1985, Honolulu, HI, p 82.

4. "The Stratocumulus Nature of Fog" by R. W. Welch and B. A. Wielicki. IAMAP/IAPSO Joint Assembly, 5-16 August 1985, Honolulu, HI, p 82.

4. ADVANCED DEGREES

Mr. M. G. Ravichandran has been supported by this contract. He will gradute in May, 1986, with the Master of Science degree in Computer Science from the South Dakota School of Mines and Technology.

5. BIBLIOGRAPHY

Gerber, H. E., 1981: Microstructure of a radiation fog. J. Atmos. Sci., 38, 454-458.

Jiusto, J. E., and G. G. Lala, 1983: The fog project - 1982. Preprints 9th Conf. Aerospace and Aeronautical Meteor., Omaha, NE, Amer. Meteor. Soc., _____.

Lala, G. G., J. E. Jiusto, M. B. Meyer and M. Kornfield, 1982: Mechanisms of radiation fog formation on four consecutive nights. Preprints Conf. Cloud Physics, Chicago, IL, Amer. Meteor. Soc., 9-11.

Roach, W. T., 1976: On the effect of radiative exchange on the growth by condensation of a cloud or fog droplet. Quart. J. Roy. Meteor. Soc., 102, 361-372.

_____, R. Brown, S. J. Caughey, J. A. Garland and C. J. Readings, 1976: The physics of radiation fog, Part I: A field study. Quart. J. Roy. Meteor. Soc., 102, 313-333.

Rodhe, B., 1962: The effect of turbulence on fog formation. Tellus, 14, 49-86.

APPENDIX 1

Prediction of Quasi-Periodic Oscillations in Radiation Fogs.
Part I: Comparison of Simple Similarity Approaches

R. M. WELCH AND M. G. RAVICHANDRAN

Institute of Atmospheric Sciences, South Dakota School of Mines and Technology, Rapid City, SD 57701

S. K. COX

Department of Atmospheric Science, Colorado State University, Fort Collins, CO 80523

ABSTRACT

There is considerable controversy in the literature concerning fog formation. One set of observations suggests that fog forms during a lull in turbulence, while another set of observations suggests that increased turbulence leads to fog formation.

A number of first-order closure techniques are applied to numerical simulations. The results show that fog formation and development is directly correlated with the magnitude of the eddy mixing coefficients. Larger turbulence generation leads to more rapid fog development and to larger liquid water contents. The rate at which the fog top grows is directly related to the rate at which turbulence lifts the inversion.

During the mature fog stage, a series of fog dissipation and redevelopment episodes occur. Liquid water develops in the upper regions of the fog during the turbulently quiet periods. Subsequent destabilization of the atmosphere increases turbulence generation and mixes the upper-level liquid water to the surface, creating surface fog intensification. Quasi-periodic oscillations in fog parameters are largest in the upper regions of the fog and become progressively damped in the lower regions of a thick fog.

These results are in qualitative agreement with the observations reported by Jiusto and Lala and support the hypothesis that there are distinct stages of fog development.

---

1. Introduction

During the last half-century, there have been numerous fog field programs. Fog prediction models also have grown in sophistication, but, to date, no model has r̶ ̶ ̶duced observations with any degree of satisfaction. Much of this lack of apparent progress may be traced to shortcomings of our understanding of the nocturnal boundary layer and associated parameterizations of turbulence generation. Lack of a clear understanding of how local factors, such as moisture and terrain, contribute to fog formation also hinders progress.

Generally, radiation fog forms under high pressure and stable conditions after nocturnal surface cooling lowers the temperature to the dew point. Observations in England by Roach et al. (1976) show that fog forms only after wind speeds decrease to low values, so that turbulence is nearly nonexistent. Once the fog forms, radiational cooling of the droplets causes a development and thickening of the fog.

However, the process of fog formation remains in dispute, with other observations suggesting that cessation of turbulence may not be required. Emmons and Montgomery (1947) and Fleagle (1953) have suggested that fog formation may be onset merely by the radiative cooling of air near a cold surface. On the other hand, Taylor (1917) and Rodhe (1962) suggest that fog formation is the result of the turbulent mixing of nearly saturated eddies at different temperatures. Studies of the microstructure of fog by Gerber (1981) support this hypothesis. Indeed, fog observations at Albany, New York, by Lala et al. (1982) suggest that freshening of calm winds, causing reduced stability and increased turbulence, contributes to fog formation—in apparent disagreement with those observations in England by Roach et al. (1976). Therefore, at this point in time, there is considerable uncertainty as to the processes responsible for fog formation. There have even been some reports of fogs first observed several meters off the ground, suggesting that there may be other governing factors responsible for fog formation.

Another topic of considerable interest which, as yet, has not been fully explained concerns quasi-periodic oscillations in some observed parameters. An analysis of the observations of Roach et al. (1976) by Roach (1976) showed significant phase relationships between longwave radiation, surface temperature, and wind speed that persisted for several hours. Similar short-term variations of fog parameters also have been reported by Lala et al. (1978), Gerber (1981), Lala et al. (1982) and Mason (1982). The reported periods of os-

cillation range from 10–30 min, with most observations in the range of 15–20 min. Lala et al. (1982) suggest that nights with stronger atmospheric stability have lighter winds, shorter periods of oscillation, and greater likelihood of patchy fog.

It is well known that although fog may form nearly simultaneously over large regions, there is considerable local structure in fog. Gerber (1981) found that dense fog was composed of highly structured and sharply defined local regions. Roach et al. (1976) suggest that variations in the nature and slope of the local terrain are at least partly responsible for the observed local structure. Roach (1976) attributes the quasi-periodic oscillations to gravity waves propagating at the top of the boundary layer. He establishes a rule-of-thumb that variations caused by advection are on the order of 5–10 min, while the longer quasi-periodic oscillations are controlled by a fluctuating balance between radiation cooling and turbulent diffusion.

Landsat very high spatial resolution digital data have been analyzed for selected fog episodes. In each case, the fog was found to be composed of cellular elements with the fog resembling a stratocumulus cloud. An analysis of the sizes of these cellular elements is given by Welch and Wielicki (1986). The possibility exists that advection of these cells across the site may contribute to at least some of the observed variation. Choularton et al. (1981) found pronounced periodic fluctuations in liquid water content with periods on the order of 70 s, possibly associated with convective motions in the form of Benard cells.

To date, fog models have not been successful in predicting quasi-periodic oscillations. One purpose of the present paper is to demonstrate that even simple similarity theory approaches for the parameterization of turbulent mixing are capable of simulating such behavior.

Due to their inherent simplicity, and also due to the fact that such approaches are computationally less expensive than higher-order closure techniques, similarity-theory parameterizations are widely used in the meteorology community. Indeed, a number of studies have shown that similarity approaches at least approximately simulate the boundary layer exchange processes; for instance, see Panofsky and Dutton (1984).

While similarity approaches may provide a reasonable simulation of turbulent mixing in clear air, it is questionable whether or not such approaches are adequate in fogs. As a fog develops, radiational cooling shifts from the ground to the fog top, thereby causing the surface inversion to lift. The establishment of superadiabatic lapse rates near the ground with weak convective motions (Mason, 1982) often is associated with fog development. Later, these superadiabatic lapse rates may be found near the fog top (Jiusto and Lala, 1983a). Clearly, methods that calculate Obukhov lengths and Richardson numbers based upon layer averages near the surface are incapable of simulating such

complicated vertical structure. Brown and Roach (1976) suggest that the constant flux layer may only be a few meters deep in fogs, with patchy regions of turbulence above this layer.

Nevertheless, and in spite of these limitations, it is perhaps surprising to see how well stability-corrected versions of similarity theory are able to produce fog temperature and liquid water profiles that are in qualitative agreement with observations. At present, there have been no detailed comparisons between higher-order turbulence formulations and fog observations. Indeed, due to the sparsity of turbulence measurements in fogs, there is great uncertainty as to the proper parameterization of various coefficients required in the higher-order closure formulations. It has not been demonstrated that more sophisticated approaches will actually produce better agreement with observations, even though this is certainly expected.

The present paper applies a number of stability-corrected turbulent exchange methods to simulate fog formation, demonstrates that these approaches do predict quasi-periodic oscillations in fog parameters, and analyzes the interaction of radiational cooling and turbulent mixing. A later paper (Part II) will apply local Richardson number approaches and higher-order closure methods. Comparison among the various approaches and with observations can then determine the cost effectiveness of the more sophisticated methods. If it should be demonstrated that these other approaches only marginally improve the agreement with observations, then that should be a clear sign that the importance of other factors such as wetness, vegetation, the slope of the ground, local topography, and pollution need to be more fully addressed (Mason, 1982).

2. Observations

The observations at Albany, New York, identified five distinct stages in the evolution of a dense fog (Jiusto and Lala, 1983a).

a. Sundown stage

The surface layer was observed to change from a lapse condition just before sunset (1800 LST) to a strong temperature inversion structure (7°C/16 m) by 2000 LST.

b. Conditioning stage

This second period lasted from 6 to 9 hours, with surface layer cooling decreasing throughout the period to about 1°C h⁻¹. Cooling was observed to propagate to higher levels as heat was lost by downward turbulent flux to the cold surface and radiative fluxes upward. Relative humidity increased (up to a height of 16 m) to values in excess of 97% during this period. Highly oscillatory behavior in visibility, relative humidity, and drop concentrations was observed.

c. Mature stage

Dense fog showed variable oscillations in the observed variables, but they became highly damped. Quasi steady-state conditions prevailed during this stage. Vertical temperature structure tended to range between isothermal conditions near the ground to even superadiabatic lapse rates.

d. Sunrise stage

The dense ground fog was observed to become more intense shortly after sunrise. Reformation of the fog was observed to occur after sunrise in other cases.

e. Fog dissipation stage

Radiation fog typically "burns off" within 2–4 hours after sunrise, predominantly due to heating of the ground and increased turbulent mixing with dry air from aloft.

3. The fog model

The model simulations reported in section 4 are compared to the various stages of fog formation listed in section 2. It is shown that the numerical model predicts these five fog stages.

a. Mathematical formulism

1) ATMOSPHERIC PROGNOSTIC EQUATIONS

Potential temperature, humidity, liquid water, pollution concentration, and wind vertical profiles in the boundary layer, respectively, are assumed to be described by the set of one-dimensional equations listed here (Roach et al., 1976; Forkel et al., 1984):

$$\frac{\partial \theta}{\partial t} = \frac{\partial}{\partial z}\left(K_h \frac{\partial \theta}{\partial z}\right) - \frac{(P_0/P)^\kappa}{\rho c_p}\frac{\partial F_N}{\partial z} + \frac{(P_0/P)^\kappa L_v}{c_p} C + \psi_h \tag{1a}$$

$$\frac{\partial q}{\partial t} = \frac{\partial}{\partial z}\left(K_q \frac{\partial q}{\partial z}\right) - C \tag{1b}$$

$$\frac{\partial w_l}{\partial t} = \frac{\partial}{\partial z}\left(K_w \frac{\partial w_l}{\partial z}\right) + \frac{\partial G}{\partial z} + C \tag{1c}$$

$$\frac{\partial \rho^{aer}}{\partial t} = \frac{\partial}{\partial z}\left(K_{aer} \frac{\partial \rho^{aer}}{\partial z}\right) + \psi_{aer} \tag{1d}$$

$$\frac{\partial V_H}{\partial t} + f\mathbf{k} \times V_H = f\mathbf{k} \times V_g + \frac{\partial}{\partial z}\left(K_m \frac{\partial V_H}{\partial z}\right) \tag{1e}$$

where

z, t	height coordinate, time
θ	potential temperature
q, w_l	humidity mixing ratio, liquid water
ρ, ρ^{aer}	air density, partial density (concentration of dry aerosol)

C	rate of condensation per unit mass of air
G	gravitational settling flux of liquid water
$K_h, K_m, K_q,$ K_w, K_{aer}	microturbulent diffusion coefficients for fluxes of heat, momentum, humidity, liquid water and aerosol
$V_H = u, v$	horizontal wind
$V_g = U_g, V_g$	geostrophic wind
f	Coriolis parameter
$\mathbf{k}$	vertical unit vector
P, P_0	air pressure, standard air pressure
κ	Poisson's constant
F_N	net flux of short- and longwave radiation
c_p	heat capacity of air at constant pressure
L_0, L_v	Obukhov length, latent heat
ψ_h, ψ_{aer}	heat and pollution sources.

2) DIAGNOSTIC EQUATIONS

The present formulism does not allow for supersaturated conditions, does not solve the droplet growth equation, and does not use aerosol particles as condensation nuclei. Rather, the McDonald (1963) saturation adjustment procedure is invoked to account for latent heat release and liquid water formation. Brown (1980) shows that differences in the predicted fog development between the drop growth procedure and the saturation adjustment method are not large.

Following Brown and Roach (1976), the gravitational flux of droplets is approximated by

$$G = V_T w_l \tag{2}$$

where V_T is the average droplet terminal velocity. The linear regression model of Brown and Roach (1976) is used to parameterize V_T (m s^{-1}) as

$$V_T = 0.0625 w_l \tag{3}$$

for liquid water contents ranging up to $w_l = 0.3$ g m^{-3}, as typically found in fogs.

At relative humidities below 100%, water vapor condenses on aerosol particles, forming a thin mist. This process is included by assuming a Junge-type particle distribution, using Hanel's (1976) method for relative humidities below 99.8% to compute the equilibrium radii. For relative humidities between 99.8% and 100.0%, the size distribution of the haze particles is based on the results of Neiburger and Chien (1960).

b. Radiative transfer

The generalized two-stream approximation of Zdunkowski et al. (1982) is used to compute radiative fluxes and heating/cooling rates. The parameterization of absorption and extinction coefficients for both the solar and infrared window spectral regions is given by Forkel et al. (1984). Multiple scattering by particles and droplets is ignored in the strong infrared absorption bands of water vapor and carbon dioxide. However, an extended emissivity method is used to account for

overlapping absorption effects of gases, particles, and droplets.

c. The Brunt-Väisälä frequency

A number of parameterizations, including the Richardson number and scale length, depend upon the value of the Brunt-Väisälä frequency, N. For unsaturated air,

$$N^2 = \frac{g}{\theta}\frac{d\theta}{dz} = \frac{g}{T}\left(\frac{dT}{dz} + \Gamma_d\right). \qquad (4)$$

For saturated air, a number of expressions have been suggested (Dudis, 1972; Fraser et al., 1973; Lalas and Einaudi, 1974; Durran and Klemp, 1982). Lalas and Einaudi (1974) give the form

$$N_m^2 = \frac{g}{T}\left(\frac{dT}{dz} + \Gamma_m\right)\left(1 + \frac{L_v q_s}{RT}\right) - \frac{g}{1 + q_w}\frac{dq_w}{dz}, \qquad (5)$$

where R is the dry air gas constant, Γ_m is the saturated adiabatic lapse rate, and q_w, the total water mixing ratio, is the sum of the saturation mixing ratio, q_s, and the liquid water mixing ratio, q_l. However, the above expression can be difficult to evaluate numerically. Durran and Klemp (1982) show that a very good approximation to Eq. (5) is

$$N_m^2 = g\left\{\frac{1 + (L_v q_s/RT)}{1 + (\epsilon L_v^2 q_s/C_p RT^2)}\right.$$

$$\left. \times \left(\frac{d\ln\theta}{dz} + \frac{L_v}{C_p T}\frac{dq_s}{dz}\right) - \frac{dq_w}{dz}. \qquad (6)\right.$$

d. Turbulence formulations

While there has been some success in modeling the unstable boundary layer, an effective parameterization for turbulent exchange remains elusive for the nocturnal stable boundary layer. The proven and tested state-of-the-art has not progressed much beyond K-type theories (Blackadar, 1979). As there have been no serious efforts to measure turbulent variances and covariances under saturated conditions, it is necessary to assume that those formulations developed for unsaturated conditions apply equally well to fogs. It is assumed that turbulence is continuous, not intermittent (Kondo et al., 1978), that there are no terrain effects (Brost and Wyngaard, 1978), and that gravity waves are not present (Finnigan and Einaudi, 1981).

A number of different turbulent exchange formulations are applied, each based either upon measurements or upon simplifications of second-order closure approximations. The first two methods are based upon stability corrections to expressions appropriate for neutral conditions (superscript n):

$$K_{m,h} = \frac{K_{m,h}^n}{\phi_{m,h}} + K_0. \qquad (7)$$

where subscripts m and h refer to momentum and heat fluxes, respectively, the $\phi_{m,h}$ are the Monin-Obukhov profile functions, and K_0 is a background or molecular diffusivity term below which the eddy diffusivity coefficients are not allowed to fall (Zhang and Anthes, 1982): $K_0 = 2.4 \times 10^{-5}$ m^2 s^{-1}. The first of these formulations is due to Shir (1973)

$$K_m^n = \frac{kzu_*}{2}\left\{\exp\left(\frac{-4z}{h}\right) + \frac{1}{1 + 16\left(\frac{z}{h}\right)^{1.6}}\right\}, \qquad (8)$$

and the second is due to Blackadar (1962)

$$K_m^n = l^2 s \qquad (9)$$

where h is the height of the boundary layer, l is the mixing length, and

$$s = \left[\left(\frac{\partial u}{\partial z}\right)^2 + \left(\frac{\partial v}{\partial z}\right)^2\right]^{1/2}. \qquad (10)$$

There is considerable controversy surrounding the parameterization of both h and l (Zilitenkevich, 1972; Delage, 1974; Wyngaard, 1975; Brost and Wyngaard, 1978; Blackadar, 1979; Arya, 1981; Andre and Mahrt, 1982; Nieuwstadt, 1984). The height of the boundary layer is parameterized (Brost and Wyngaard, 1978) as

$$h = d(u_* L_0/f)^{1/2} \qquad (11)$$

with $d = 0.40$, in agreement with Zilitenkevich (1972, 1975), and L_0 the Obukhov length. However, the value of d depends upon the wind direction relative to a slope, the angle of the sloping surface, and the surface cooling rate (Brost and Wyngaard, 1978). Furthermore, under stable conditions, the breakdown from turbulent to laminar flow may occur at very low levels (Businger and Arya, 1974), with alternating layers of weakly turbulent and laminar flow aloft (Xing-Sheng et al., 1983).

The variable mixing length is often expressed (Blackadar, 1979) as

$$l = k(z + z_0)/[1 + k(z + z_0)/\lambda]. \qquad (12)$$

Near the surface, the height z is the proper scaling length, but when $z > L$, Businger and Arya (1974) and Blackadar (1979) suggest that $l = L$ may be appropriate.

$$l = \begin{cases} z, & z < L_0 \\ L, & z \geq L_0. \end{cases} \qquad (13)$$

An alternate expression is suggested by Brost and Wyngaard (1978) in the form

$$\frac{1}{l} = \frac{1}{z} + \frac{1}{l_B} \qquad (14)$$

where l_B is the buoyancy length scale.

$$l_B = C_B \frac{\sigma_*}{N} \qquad (15)$$

with $C_B = 1.69$. In a fog, N is replaced with N_m (Eq. 6). The value of σ_w is from Nieuwstadt (1984),

$$\sigma_w = 1.4\mu_*[1 - z/h]^{3/4}. \tag{16}$$

Equations (13) and (14) express the fact that in a stable boundary layer, the turbulent eddy is restricted so that turbulence no longer "feels" the presence of the surface (Nieuwstadt, 1984).

The Monin-Obukhov stability functions [Eq. (7)] also need to be specified. However, once again there is considerable controversy as to which expressions are most appropriate (Blackadar, 1979). We consider the following three forms.

1) Businger et al. (1971):

unstable conditions

$$\phi_m = (1 - 15\zeta)^{-1/4}$$

$$\phi_h = (1 - 9\zeta)^{-1/2} \tag{17}$$

stable conditions

$$\phi_m = 1 + 4.7\zeta$$

$$\phi_h = 0.74 + 4.7\zeta,$$

where $\zeta = z/L_0$. \hfill (18)

2) Carl et al. (1973):

unstable conditions

$$\phi_m = (1 - 15\zeta)^{-1/3}$$

$$\phi_h = 0.74(1 - 16\zeta)^{-1/2}$$

stable conditions

$$\phi_m = 1 + 5\zeta$$

$$\phi_h = \begin{cases} 0.74 + 9.6\zeta + 29.6\zeta^2 & \zeta < 0.08 \\ 1.2 + 6.1\zeta & \zeta \geq 0.08. \end{cases} \tag{19}$$

3) Dyer and Bradley (1982):

unstable conditions

$$\phi_m = (1 - 28\zeta)^{-1/4}$$

$$\phi_h = (1 - 28\zeta)^{-1/2}$$

stable conditions

$$\phi_h = \phi_m = 1 + 4.7\zeta. \tag{20}$$

We also consider a few other parameterizations for turbulent mixing in the steady-state, stable boundary layer. Businger and Arya (1974) suggest the following form for turbulent mixing coefficients of momentum,

$$K_m = \frac{ku_*z \, \exp(-V_g fz/u_*^2)}{1 + 4.7\zeta} + K_0. \tag{21}$$

Here we take $K_h = K_m$ for the stable case and use Blackadar's (Eq. 9) exchange with Businger et al.'s (1971) stability (Eq. 17) for unstable conditions.

Based upon a simplified version of Wyngaard's (1975) second-order turbulence for the stable boundary layer, Brost and Wyngaard (1978) suggest the following form

$$K_m = \frac{ku_*h\left(\dfrac{z}{h}\right)\left(1 - \dfrac{z}{h}\right)^{1.5}}{1 + 4.7\left(\dfrac{z}{h}\right)\left(\dfrac{h}{L_0}\right)} + K_0 \tag{22}$$

with $K_h = 1.25K_m$.

In contrast, Panofsky and Dutton (1984) suggest the very simple form for stable air,

$$K_h = K_m = \frac{ku_*z}{\phi_m} + K_0. \tag{23}$$

Based upon second-order closure, Blackadar (1979) suggests that for unstable conditions,

$$\left.\begin{array}{l} K_m = l^2s(1 - 21 \, \text{Ri})^{1/2} \\ K_h = l^2s(1 - 87 \, \text{Ri})^{1/2} \end{array}\right\} \tag{24}$$

and for stable conditions,

$$K_h = K_m = \begin{cases} 1.1 \dfrac{\text{Ri}_c - \text{Ri}}{\text{Ri}_c} l^2s, & \text{Ri} \leq \text{Ri}_c \\ 0, & \text{Ri} \geq \text{Ri}_c. \end{cases} \tag{25}$$

For both the Brost and Wyngaard exchange (22), and the Panofsky and Dutton exchange (23), we use Eq. (24) for unstable conditions.

e. The Richardson number

Following Blackadar (1979), the Richardson number Ri is calculated rather than Obukhov length L_0. The Richardson number is expressed for unsaturated conditions [Eq. (4)] as

$$\text{Ri} = N/s, \tag{26}$$

and for saturated conditions (Eq. 6) as

$$\text{Ri} = N_m/s. \tag{27}$$

The similarity function may be obtained from Businger et al. (1971)

for unstable conditions

$$\text{Ri} = \frac{0.74\zeta(1 - 15\zeta)^{1/2}}{(1 - 9\zeta)^{1/2}} \tag{28}$$

and for stable conditions

$$\text{Ri} = \frac{\zeta(0.74 + 4.7\zeta)}{(1 + 4.7\zeta)^2}. \tag{29}$$

However, Panofsky and Dutton (1984) note that simpler relationships given by Businger (1966) and Pandolfo (1966) differ significantly only in nearly neutral conditions and are not necessarily less accurate than Eqs. (28)-(29).

For unstable air

$$\zeta = \text{Ri}. \qquad (30)$$

For stable air

$$\zeta = \frac{\text{Ri}}{1 - 5\,\text{Ri}}. \qquad (31)$$

The present calculations use a mixture of these two approaches, inverting Eq. (29) for stable conditions and using a simplified version of Eq. (28)

$$\text{Ri} = 0.74\zeta \qquad (32)$$

for unstable conditions.

f. Soil equations

The equations for heat and moisture transport in the soil are given by

$$(C_s + lb)\frac{\partial T_s}{\partial t} + la\rho_w \frac{\partial \eta}{\partial t} + \frac{\partial}{\partial z}\left(-\lambda_T \frac{\partial T_s}{\partial z} + T_s \frac{\partial \psi}{\partial T} J_w\right)$$

$$+ l\frac{\partial}{\partial z} J_v = -J_v\left(\frac{\partial h_v}{\partial z} + g\right)$$

$$- J_w\left(\frac{\partial h_w}{\partial z} + g\right) + (\eta_p - \eta)\frac{\partial P}{\partial t} \qquad (33)$$

$$\rho_w(1 + a)\frac{\partial \eta}{\partial t} + b\frac{\partial T_s}{\partial t} = -\frac{\partial}{\partial z}(J_v + J_w) \qquad (34)$$

with

C_s, T_s specific heat of soil at constant pressure, soil temperature

l, λ_T heat of evaporation of water in soil, thermal conductivity

ρ_w, η, η_p density of water, liquid water content of soil, porosity

ψ soil moisture potential

J_v, J_w fluxes of water vapor and liquid water in soil

h_v, h_w partial specific enthalpy for water vapor and liquid water

a, b, c parameters given by Forkel et al. (1984).

The moisture potential ψ results from capillary and adsorption effects and is a function of both temperature and soil liquid water. Equations (33–34) are a coupled pair involving heat conduction, phase change and transport. A complete description of the soil model is found in Forkel et al. (1984) and Sievers et al. (1983).

g. Interface conditions

The atmosphere and soil system are coupled at the soil surface by interface conditions of heat and water:

$$F_n - \rho C_p K_h \frac{\partial \theta}{\partial z} + \lambda_T \frac{\partial T_s}{\partial z}$$

$$+ \left(-\rho K_h \frac{\partial q}{\partial z} - J_v\right)(L_v - \psi) = 0 \qquad (35)$$

$$-\rho K_n \frac{\partial \eta}{\partial z} - J_v - J_w = 0, \qquad (36)$$

where J_v and J_w are the soil fluxes of water vapor and liquid water, respectively. The saturation vapor pressure of water in soil is

$$P_s{}^s = P_s \exp\left(\frac{\psi}{R_v T_s}\right), \qquad (37)$$

where P_s is the saturation vapor pressure of a flat water surface and R_v is the water vapor gas constant. Temperature, liquid water, and vapor may be determined at the soil interface using Eqs. (35–37). Note that sedimentation of fog droplets is assumed to contribute to dew formation, but not to the soil interface conditions. The upward-directed water vapor flux from the soil also contributes to dew formation (Monteith, 1957).

h. Boundary conditions

The upper and lower boundary conditions are taken as

$$\left.\begin{array}{l} u = u_g, \quad v = 0 \\[4pt] \dfrac{\partial \theta}{\partial z} = 0.35°\text{K}/100 \text{ m} \\[8pt] \dfrac{\partial q}{\partial z} = \alpha q_{n-1} \\[8pt] \dfrac{\partial \rho^{\text{aer}}}{\partial z} = 0 \end{array}\right\} \quad \text{at} \quad z = 3 \text{ km}, \qquad (38)$$

$$w_l{}^{\text{top}} = 0 \quad \begin{array}{l}\text{at first grid point above the fog} \\ \text{with relative humidity} < 100\%,\end{array} \qquad (39)$$

$$u, v = 0 \quad \text{at} \quad z = z_0, \quad \text{roughness height}, \qquad (40)$$

and

$$\left.\begin{array}{l} T_s = \text{constant} \\[4pt] w_l{}^s = \text{constant} \end{array}\right\} \quad \text{at} \quad z = -1 \text{ m in soil}. \qquad (41)$$

Here q_{n-1} refers to the mixing ratio one grid point below the upper boundary; u_g is the geostrophic wind.

i. The numerical procedure

The numerical evaluation is carried out using an implicit scheme. For higher resolution of the grid near the soil surface, the basic equations are subjected to logarithmic and square root transformations in the air and within the soil, respectively. Details are given by Zdunkowski et al. (1976). The maximum possible time step during fog episodes is determined by droplet settling. Integration time steps of 1 s are required. In the absence of fog, 75 s time steps are used.

j. Initial conditions

The numerical simulations reported below refer to early October at Albany, New York. Prediction begins

at 1800 (local time used throughout) and continues until 1000 the next morning.

The present study attempts to simulate the observations of Jiusto and Lala (1983a,b), Jiusto and Lala (1982), and Lala et al. (1982) in October of 1981 and 1982. While a complete dataset is not available from these reports, a representative vertical temperature structure is taken from these studies for the lower 16 m. No information is available above this height. Surface temperature at 1800 is taken to be 14°C, decreasing to 12°C at a height of $z = 0.1$ m. The atmosphere is assumed to be isothermal at 12°C up to a height of $z = 0.5$ km, decreasing to 11°C at $z = 1$ km and to -3°C at $z = 3$ km. Soil temperature is assumed to increase to 15.5°C at a depth of $z = -5$ cm, and then to gradually decrease to 15°C at a depth of $z = 1$ m.

Relative humidity U (in percent) is assumed to be $U = 80$ up to a height of $z = 0.5$ km, then decreasing linearly with height to $U = 60$ at $z = 3$ km. Above that height, the average observed autumnal values are used for calculating the radiative transfer. Soil moisture is assumed to be $\eta = 0.16$ at the surface, increasing to $\eta = 0.2$ at a depth of $z = -1$ m. Data for soil moisture potential and hydraulic conductivity are taken from Hillel and van Bavel (1976), and thermal conductivity is given by Baver et al. (1972). Geostrophic wind is taken for calm conditions as 2 m s^{-1} and the roughness height z_0 is taken as 1 cm. Weak pollution is assumed, with ground concentration of 5000 aerosol particles/cm^3, corresponding to a visibility of 60 km at $U = 50$. The initial particle distribution is assumed to decrease exponentially with height as $\exp(-z/H_D)$ where H_D is taken as 1 km.

4. Results

a. Color processed display of results

Figure 1 shows a color processed display of temperature, liquid water content, heating/cooling rate, and eddy mixing. The horizontal coordinate is local time and the vertical coordinate is height. Even though fog extended to heights of 200-300 m in the early morning hours, only the lower 150 m is shown in this figure. This choice represents a compromise in limiting the coverage of the upper region of the fog in order to improve the resolution near the ground. Soil temperature in the first meter below the surface is included in the first frame. A color code is found below each of the individual frames to convert the colors to the appropriate numerical values. For instance, yellow represents liquid water content in the range 0.15–0.20 g m^{-3} (second frame). However, use of only eight temperature classifications (i.e., colors) is found to be insufficient to fully visualize the temperature variations. Therefore, a more detailed color scheme is used, as shown in Frame 1.

It should be noted that color image display contains a higher information content than standard methods of presenting results. Therefore, taking time to become familiar with the rainbow color scheme is advised before proceeding to discussion of the results. Note that the black and blue colors generally represent the smallest values and the red and white colors represent the largest values.

b. Businger-Arya exchange

This section discusses the development of fog as predicted using the Businger-Arya (1974) eddy exchange formulation [Eq. (25)] using the Businger et al. (1971) stability coefficients [Eq. (21)]. Scaling length is given by Eq. (15), and the height of the boundary layer is calculated from Eq. (11). Comparison is made with the observations of Jiusto and Lala (section 2) to determine how well the model simulates the observed stages of fog development.

1) SUNDOWN STAGE

Surface temperature decreases rapidly during the first two hours of simulation, dropping from 14°C at 1800 to 9.7°C at 1900 and to 8°C at 2000. Due to the large changes in temperature in the lower meter of the atmosphere and the pixel resolution limitations of the color imaging system, it is difficult to obtain accurate surface temperatures in Fig. 1a. Above the surface, at heights of 1–10 m, the decrease in temperature is much more gradual, with a cooling of 0.5°C h^{-1}. These values are much smaller than the 7°C h^{-1} decrease in surface temperature and the 4–6°C h^{-1} change in the 0.5–16 m layer observed by Jiusto and Lala (1983a).

The height of the boundary layer (Fig. 2a) decreases from its original $h = 85$ to 60 m at 1900 and then rapidly drops to just a few meters at 2000. During this initial stage, radiative cooling of the surface (Fig. 2b) is dominant, with turbulent transport suppressed due to the presence of the strong surface inversion (Fig. 2c).

2) CONDITIONING STAGE

During the next four hours, surface cooling decreases by a relatively uniform 1°C h^{-1} to 4.2°C at 2400 (Fig. 1a). This rate of decrease is similar to that observed by Jiusto and Lala. During this period, the surface inversion increases in intensity and in height (Figs. 1a and 2a). By 2400, the inversion is 6.5°C/50 m. After the collapse of the height of the boundary layer at 2000, the gradual increase in surface stress causes a decrease in stability (Ri < Ri$_c$, Fig. 2c), a gradual increase in the height of the boundary layer (Fig. 2a), and increased turbulent mixing (Fig. 1d). Increased mixing then leads to increased cooling at higher levels as heat is transported to the ground to be radiated to space.

The region below the top of the inversion now begins to show rapid increases in relative humidity. However, above this region of turbulent mixing, relative humidity changes slowly. This demonstrates that during this conditioning stage, the loss of energy to the ground by turbulent transport is an order of magnitude more im-
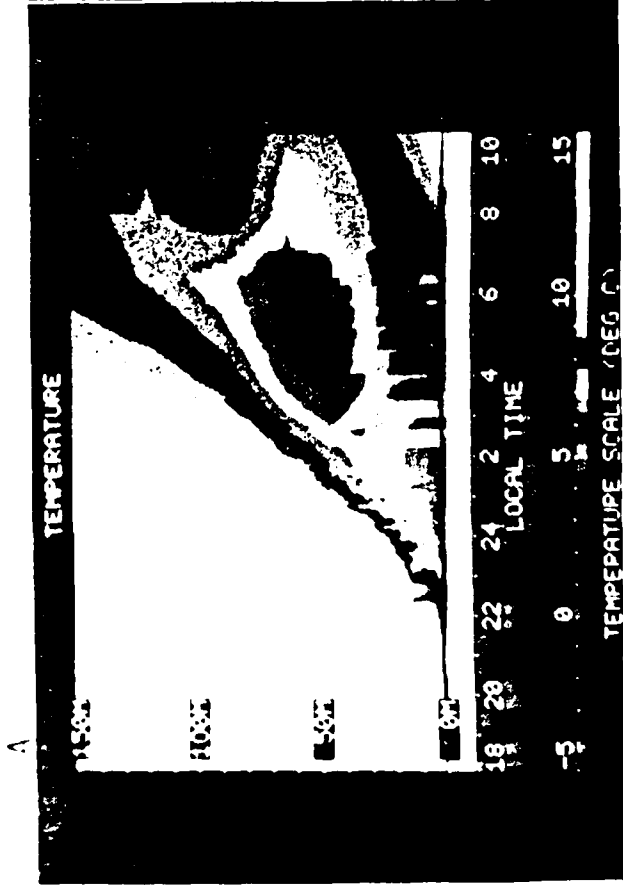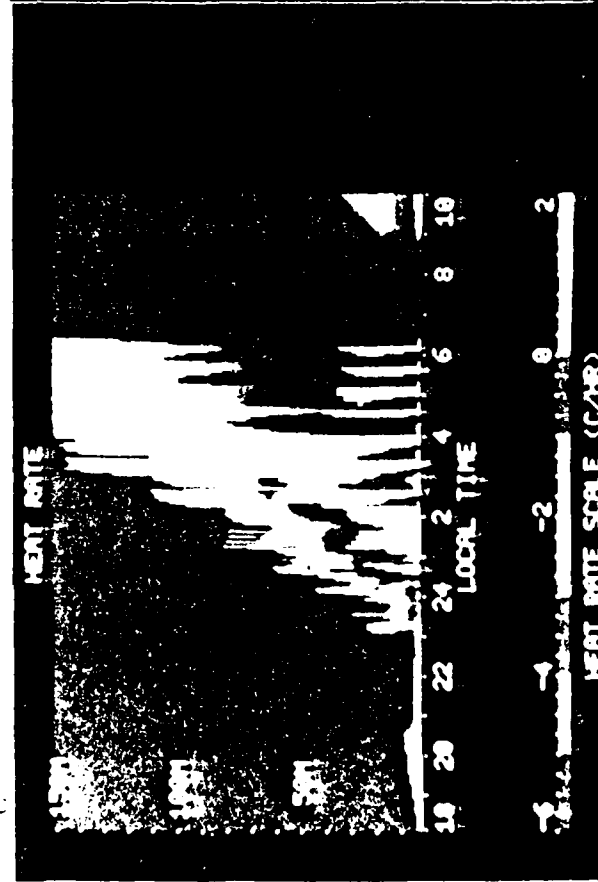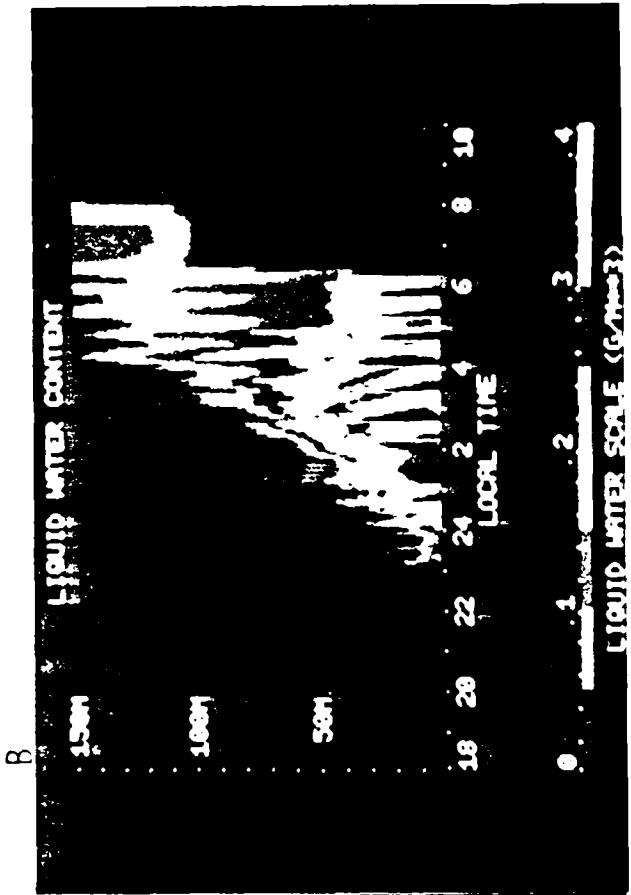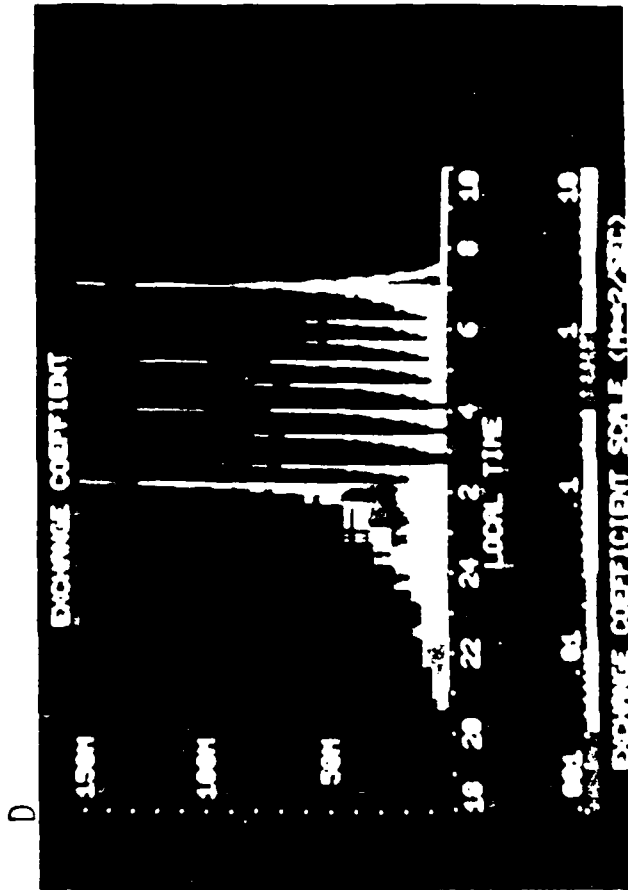
Fig. 1 Temperature, liquid water content, heating/cooling rate, and eddy exchange coefficient as a function of height and local time using the Businger-Arya turbulence formulation
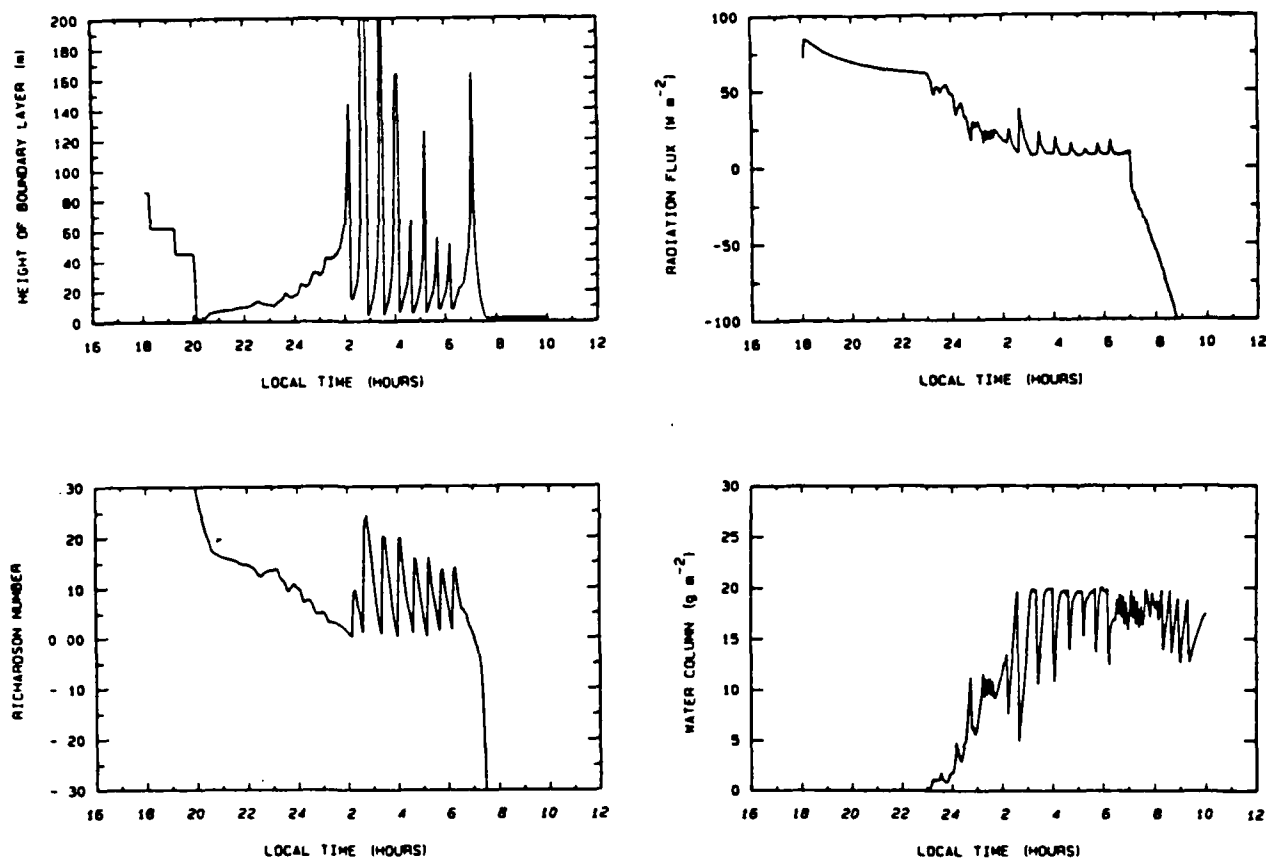
FIG. 2. (a) Height of the boundary layer, h; (b) radiation flux at the surface; (c) Richardson number, Ri; and (d) water column as a function of height and local time using the Businger-Arya turbulence formulation.

portant than is the loss of energy by radiative cooling. Similar behavior is observed by Jiusto and Lala. By 2300, relative humidity exceeds 99% to a height of 10 m.

At 2300, the eddy exchange coefficient decreases slightly in magnitude and then intensifies (Figs. 1d and 2c). It is at this point that the fog forms. For the next 45 min, the ground fog oscillates in height between 10 and 20 m, with a periodicity of 20–30 min (Figs. 1b and 2d). Liquid water content averages about $w_l = 0.05$ g m^{-3} near the fog top to about 0.15 g m^{-3} near the ground. Radiative cooling rates are strongly correlated with liquid water content in this shallow ground fog, ranging from $-2°C$ h^{-1} near fog top to almost $-5°C$ h^{-1} near the ground.

3) MATURE FOG STAGE

During the next two hours (until 0200), the turbulent mixing coefficients rapidly increase in intensity and height (Fig. 1d) as atmospheric stability decreases (Fig. 2c) and the height of the boundary layer increases (Fig. 2a). The increase in fog height and fog liquid water content is directly correlated with the increase in tur-

bulence. This turbulent region continues to experience large values of heat transport to the ground. During this period, the region of maximum radiational cooling lifts off the ground into the upper regions of the fog. Radiational cooling rates on the order of $-3°C$ h^{-1} to $-4°C$ h^{-1} are common (Fig. 1c).

Near the ground, liquid water content slowly increases to about 0.25–0.3 g m^{-3}, being relatively uniform with height in the lower 20 m. However, liquid water is highly oscillatory in the upper regions of the fog, with fog top now reaching to about 50 m (Fig. 1b). While there is some oscillatory behavior in the liquid water content near the ground, it is highly damped.

Once fog forms and reaches a height of 10–20 m at 2400, surface IR net flux has dropped by about a factor of 2 (Fig. 2b) and surface temperature no longer decreases (Fig. 1a). At this point, the integrated vertical water column

$$w_c = \int_0^{z_T} w_l(z)dz \qquad (46)$$

is about 1–2 g m^{-2}, where z_T is the height of the fog top. At about $w_c = 2$ g m^{-2} (Fig. 2d), the surface radiative heat loss to space is balanced by downward heat

transport in the atmosphere to the surface and upward heat transport in the soil. As the fog grows thicker, the surface IR radiative loss continues to decrease (Fig. 2b) and the surface temperature begins to increase (Fig. 1a).

The behavior of the surface temperature is in agreement with the observations of Jiusto and Lala at Albany. Figure 3 shows a representative vertical temperature profile in the lower 16 m on the night of 10–11 October 1982. Note that the surface temperature increases by 2–3°C over a period of about 2.5 hours after fog forms at 0130. The atmospheric structure becomes increasingly unstable as isothermal conditions are approached at about 0400.

While the predicted temperatures are warmer than the observed temperatures shown in Fig. 3, the same behavior pattern occurs once the fog forms. The temperature structure gradually tends toward isothermal conditions in the lower 10–20 m (Fig. 1a), the Richardson number steadily decreases (Fig. 2c), and turbulent mixing coefficients increase rapidly (Fig. 1d). By 0200, a dramatic change in the fog occurs that is

not observed in the Albany field measurements. For the next four hours, the numerical simulation shows a series of pronounced oscillations in the fog parameters. With each surge in eddy mixing, the height of the boundary layer rapidly expands and contracts (Fig. 2a). When the boundary layer height increases rapidly, heat from the upper portion of the fog near the inversion top is transferred downward, and lower level moisture is mixed into the upper regions of the fog. The net effect is the rapid decrease in liquid water content in the lower 20 m of the fog from nearly $w_l = 0.3$ g m^{-3} to about $w_l = 0.01$–0.05 g m^{-3}. Above the height of 30 m, fog liquid water briefly increases to nearly $w_l = 0.4$ g m^{-3} (Fig. 1b). Air temperature in the lower 20 m increases by about 0.5–0.6°C, but surface temperature increases only by about 0.1°C (Fig. 1a). Therefore a small surface inversion forms that tends to suppress turbulent mixing (Fig. 1d; Fig. 2c).

The thick fog aloft radiatively shields the surface, preventing surface cooling. The surface warms by 0.2–0.5°C h^{-1}, while radiative cooling of the fog (−1.5 to −1°C h^{-1}) causes a gradual decrease in air temperature.
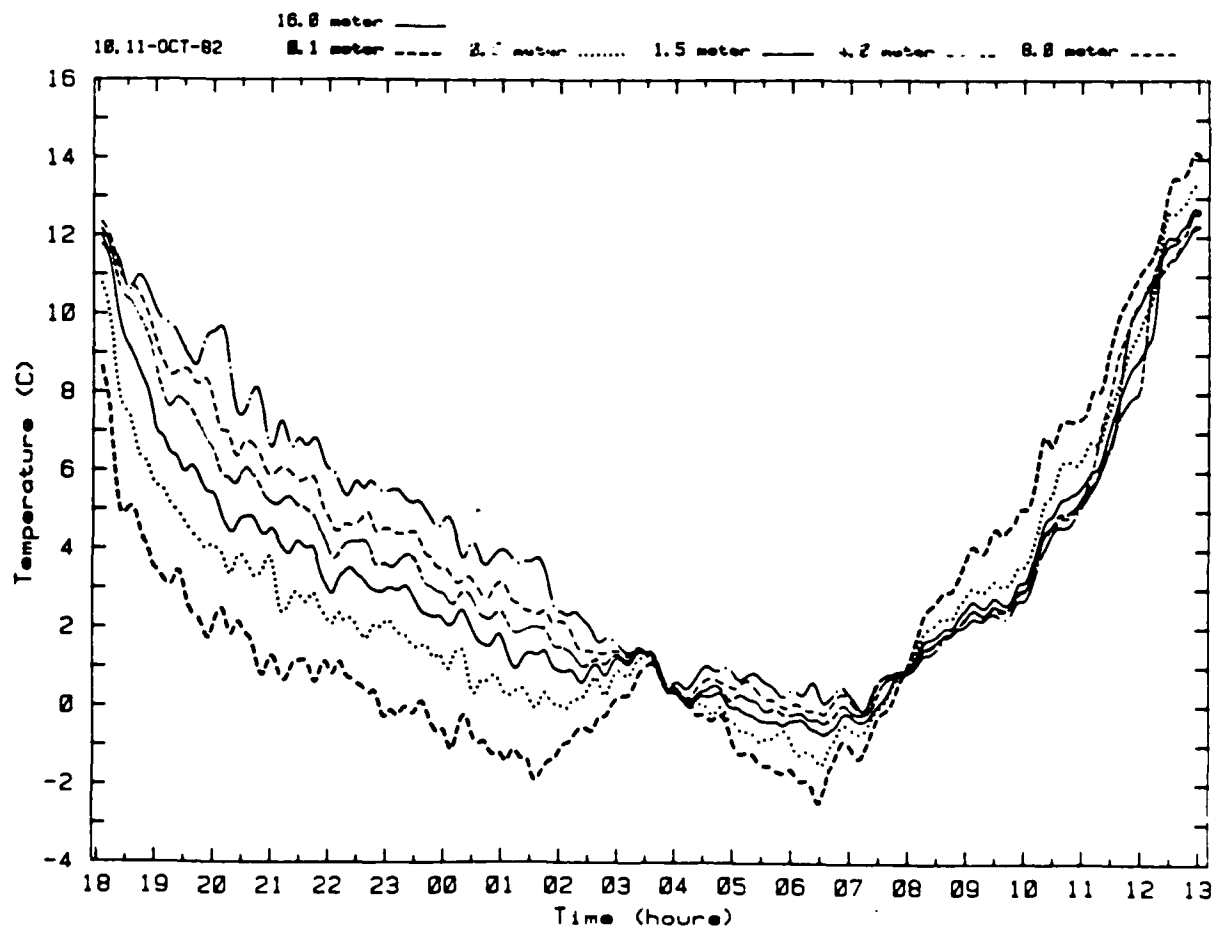

FIG. 3. Observed vertical profile of temperature as a function of local time on 10–11 October 1982 (From Jiusto and Lala, 1983a).

The net effect is the rapid breakdown of the surface inversion and the regeneration of turbulent mixing. Coupled with droplet settling, this increased turbulence causes the downward transport of liquid water from aloft, with surface values once again reaching $w_l = 0.3-0.4$ g m^{-3}.

With another surge in turbulent mixing, the cycle repeats. A series of strong quasi-periodic oscillations are produced near the ground. Above 30 m, these oscillations are less noticeable in the variation of liquid water content. However, these events act as a pumping mechanism to progressively transport moisture higher into the boundary layer. The fog top no longer increases steadily in height, but its growth is now strongly correlated with the surges in turbulent mixing. The period of oscillation found with this model is 30–40 min. In contrast, the observations show a period of light fog followed by increased fog intensity at about sunrise.

The fog continues to grow to a height of about 200 m, in agreement with the observations. The liquid water column also shows periodicity with values ranging from $w_c = 10-18$ g m^{-2} during this period. As the fog grows, dry air aloft is mixed down and gradually decreases the maximum liquid water content found near the ground. Droplet settling also contributes to a decrease in fog liquid water. In contrast to other fog models, the maximum liquid water is not always found near fog top (Fig. 1b).

4) DISSIPATION STAGE

After 0600, the moisture aloft decouples from the surface processes and a low level stratus cloud is formed from 100–225 m, with maximum liquid water content of 0.12 g m^{-3}. The presence of the stratus cloud aloft, radiatively shielding the top of the fog layer below, prevents further oscillations in the fog. The formation of a stratus layer aloft is not reported in the Albany observations.

With sunrise, the fog rapidly dissipates to a ground fog a few meters thick, with liquid water contents on the order of $w_l = 0.01-0.02$ g m^{-3}. The stratus layer top lifts to 300 m and the base lifts to about 200 m. Cloud liquid water increases to $w_l = 0.15-0.18$ g m^{-3} before gradually decreasing.

Rather than dissipating, the ground fog grows in height from about 5 m to about 10 m as dew and soil moisture are evaporated (Fig. 1b). Liquid water increases to $w_l = 0.05$ g m^{-2} at 1000 before beginning to decrease. The surface fog finally dissipates after 1030, with high relative humidity and haze persisting until 1100 (not shown).

c. Comparison with observations

Sufficient details are unavailable in the various papers reporting the Albany fog observations to make a detailed comparison with the model results. Neverthe-less the model results do predict the same stages of fog development.

The model assumes an initial temperature profile of 12°C uniform with height to 500 m, increasing to 14°C at the ground. This profile is roughly representative of the temperatures reported in the lower 16 m at 1800 on 12 October 1981 and 10 October 1982. Fog formation occurs at 2100 on 12 October 1981 and at 0100 on 10 October 1982 and at 2230 on 29 October 1981 (Fig. 4). Considering the uncertainty in the initial conditions, the predicted time of 2300 for fog formation by the model appears to be roughly comparable to observations.

Perhaps the most striking difference between model predictions and observations is the rate of temperature decrease during the "sundown" stage. Observations show a very rapid cooling of the surface layer and the eventual development of a supercooled fog. In contrast, the model predicts a much slower cooling and warm fog conditions, with a minimum surface temperature of about 4°C. This difference appears to be largely due to the rate of IR cooling in the surface layer. The following factors would lead to greater surface cooling: (i) replacement of the assumed initial temperature profile above 16 m with lapse conditions; (ii) decrease the assumed initial relative humidity profile; (iii) decrease the assumed aerosol concentration; (iv) decrease the soil conductivity; and (v) decrease the assumed initial soil temperature profile.

Figure 4 shows liquid water content measured during three different fog events at Albany. Each of these observations was made at a height of about 1.5 m. The oscillatory nature of the fog can be seen in these measurements with a period reported to be about 20 min (Jiusto and Lala, 1982; Lala et al., 1982). In addition, there seems to be a tendency for some lower frequency behavior on the order of 1–2 hours. The 29–30 October 1981 dataset is particularly interesting, showing episodes of fog development following by periods of fog dissipation near the ground.

The model predicts that periods of surface clearing often are associated with increased liquid water development near the fog top (Fig. 1b). As the present observations are only reported at shelter height, the predicted fog behavior aloft cannot be verified. However, when the detailed Albany case studies are completed and reach the literature, much more thorough comparison with the model predictions will be possible. The following studies examine to what degree the results shown in Fig. 1 are sensitive to the form of the eddy exchange formulation.

d. Richardson number

In the previous calculations, the Richardson number is computed over a height of $z = 1.5$ m, with Eqs. (29) and (32) inverted to obtain L and ζ. This is similar to $z = 0.75$ m used by Brost and Wyngaard (1978). How-
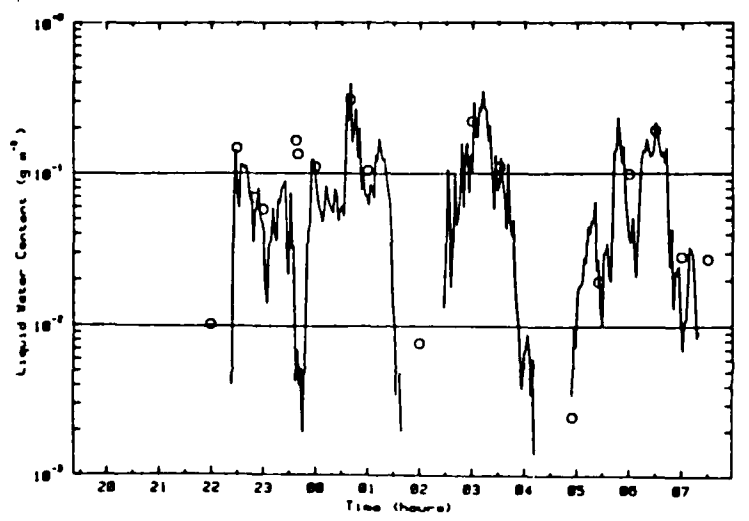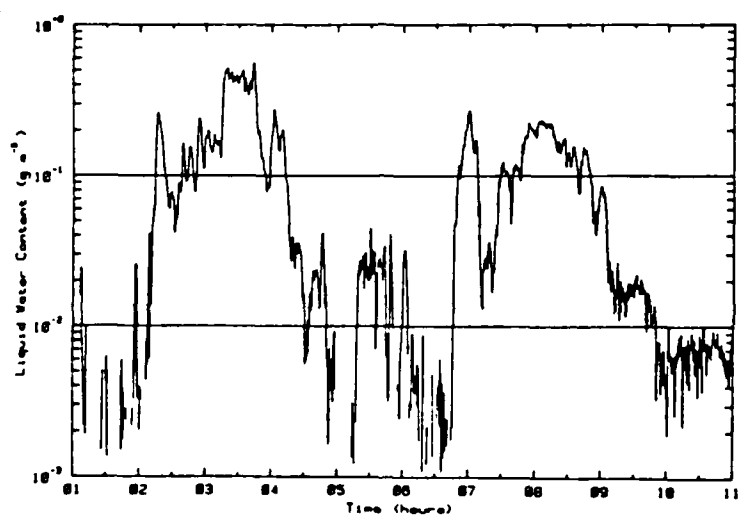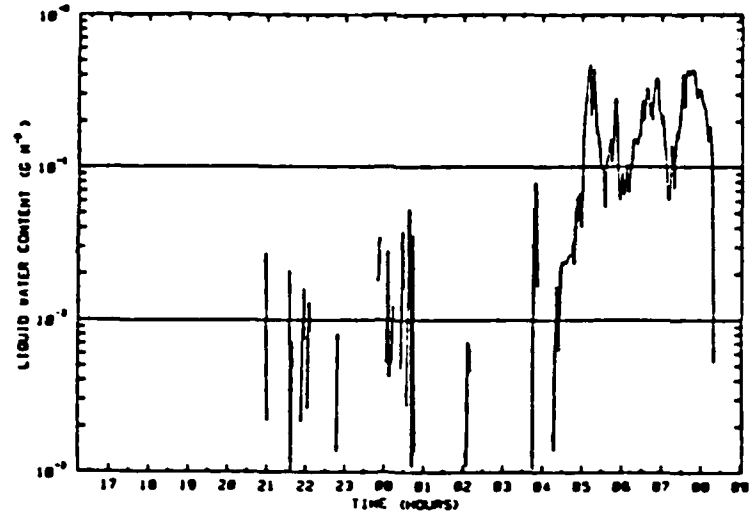
FIG. 4. Observed liquid water content at shelter height as a function of local time on: (a) 12 October 1981; (b) 10 October 1982; and (c) 29 October 1981 (From Jiusto and Lala, 1982, 1983b); Lala et al., 1982).

ever, the value of z chosen for the surface layer is somewhat arbitrary. In order to examine the sensitivity of the results to the choice of z, several different values are used.

As the value z of the surface layer is increased, the time of fog formation increases. With the choice of $z = 5$ m, fog formation is delayed nearly two hours, until 0100. A larger value of z leads to overall greater atmospheric stability and smaller eddy exchange coefficients.

The time of fog formation is directly correlated to the onset of turbulence generation. No fog is generated when turbulence is suppressed. However, as the eddy exchange coefficients exceed values of about 0.01 m² s⁻¹, then fog is formed. These results are in agreement with the observations of Jiusto and Lala (1983a) which show that increased turbulence and reduced stability contribute to fog formation.

The model predicts that the inversion lifts off the ground with development of the fog. Changes in stability are more rapid with this $z = 5$ m formulation, leading to a more rapid intensification of eddy mixing. This leads to a fog that grows in height more quickly, and one with larger liquid water content. Values of $w_l = 0.35$–0.40 g m⁻³ are now predicted for the lower 20–40 m.

The highly oscillatory behavior found in Fig. 1 remains, but the period of oscillation lengthens and the near-surface liquid water content tend to be larger. From 0330 to 0600, a series of oscillations in liquid water content occur near the surface, ranging from $w_l \approx 0.05$ g m⁻³ to $w_l \approx 0.30$ g m⁻³ with a decrease in periodicity to ~40–60 min.

e. Stability parameterizations

The previous calculations have been made using the Businger et al. (1971) Monin-Obukhov stability functions, ϕ_m and ϕ_h. However, there is considerable controversy as to which expressions are most appropriate for the nocturnal boundary layer. A rather thorough discussion is given by Blackadar (1979). Replacement of Eq. (17) with the parameterization suggested by Carl et al. (1973) given in Eq. (19) has only minor impact. The only significant difference is that the number of oscillations between 0200 and 0600 decreases from 7 (Fig. 1b) to 5; that is, the period between oscillations increases.

Replacement of Eq. (17) with the parameterization suggested by Dyer and Bradley (1982) given in Eq. (20) predicts similar behavior in the formation and mature stages. However, a sudden decrease in fog top occurs at 0400, from nearly 150 m down to 50 m. The fog then grows back to a height of 200 m by 0600. The quasi-periodic oscillations near the ground continue during the period from 0200 to 0600. Once again, the stratus cloud forms after 0600, but with somewhat larger liquid water content.

The conclusion is that the choice of stability formulation [Eqs. (17)–(20)] changes the periodicity of the oscillations somewhat, but does not affect the major stages of fog development. The time of fog formation, the development of a stratus layer after 0600, and the time of dissipation remain relatively unchanged.

f. Eddy exchange formulations

Using the Businger et al. (1971) stability functions [Eq. (17)], the eddy exchange formulations now are varied. Liquid water content, eddy exchange coefficient, and the heating/cooling rate for the Blackadar (1979) method are shown in Fig. 5a–c, respectively. Liquid water content alone is shown in Fig. 5d–f for the Brost and Wyngaard (1978), Panofsky and Dutton (1984), and Shir (1973) exchange formulations, respectively. The height of the boundary layer, the surface/radiation flux, the Richardson number, and the water column are shown for each of these four turbulent exchange methods in Fig. 6.

The processes during the sundown and conditioning stages of fog development occur at about the same rate as shown in Fig. 1 and Fig. 2. In each case, the height of the boundary collapses during the sundown stage and then gradually recovers during the conditioning stage. Fog forms between 2300 and 2400, and the initial period of fog growth is directly correlated with the strength of the turbulence generation. Cooling rates on the order of -3 to $-5°C$ h⁻¹ are common near the ground in this ground fog.

The largest liquid water content is found in those regions of the fog with the largest eddy mixing coefficients. The height of the fog top rises with increasing height of the inversion. During this stage of fog formation, the fog top height, height of the inversion, and height to which turbulence is found are all equal. This is the height of the boundary layer (Fig. 6), which is directly correlated with the top of the fog seen in the liquid water profiles (Fig. 5).

The various fog parameters show oscillatory behavior near the surface during the initial fog growth stage. This quasi-periodic variation is most evident in the Panofsky and Dutton results and least noticeable in the Shir results. However, this oscillatory behavior generally is strongest near the fog top, becoming progressively damped in the interior regions of the fog.

The Blackadar (1962) turbulent exchange formulation also has been examined (not shown in the figures). A very shallow (5–10 m) ground fog forms at 2300, which persists until 0300 before growing. The reason that this fog fails to develop over this 4 h period is that turbulence generation remains small ($K < 0.01$ m² s⁻¹). This is another confirmation that fog development during its initial growth stage is directly correlated with the strength of the eddy mixing processes.

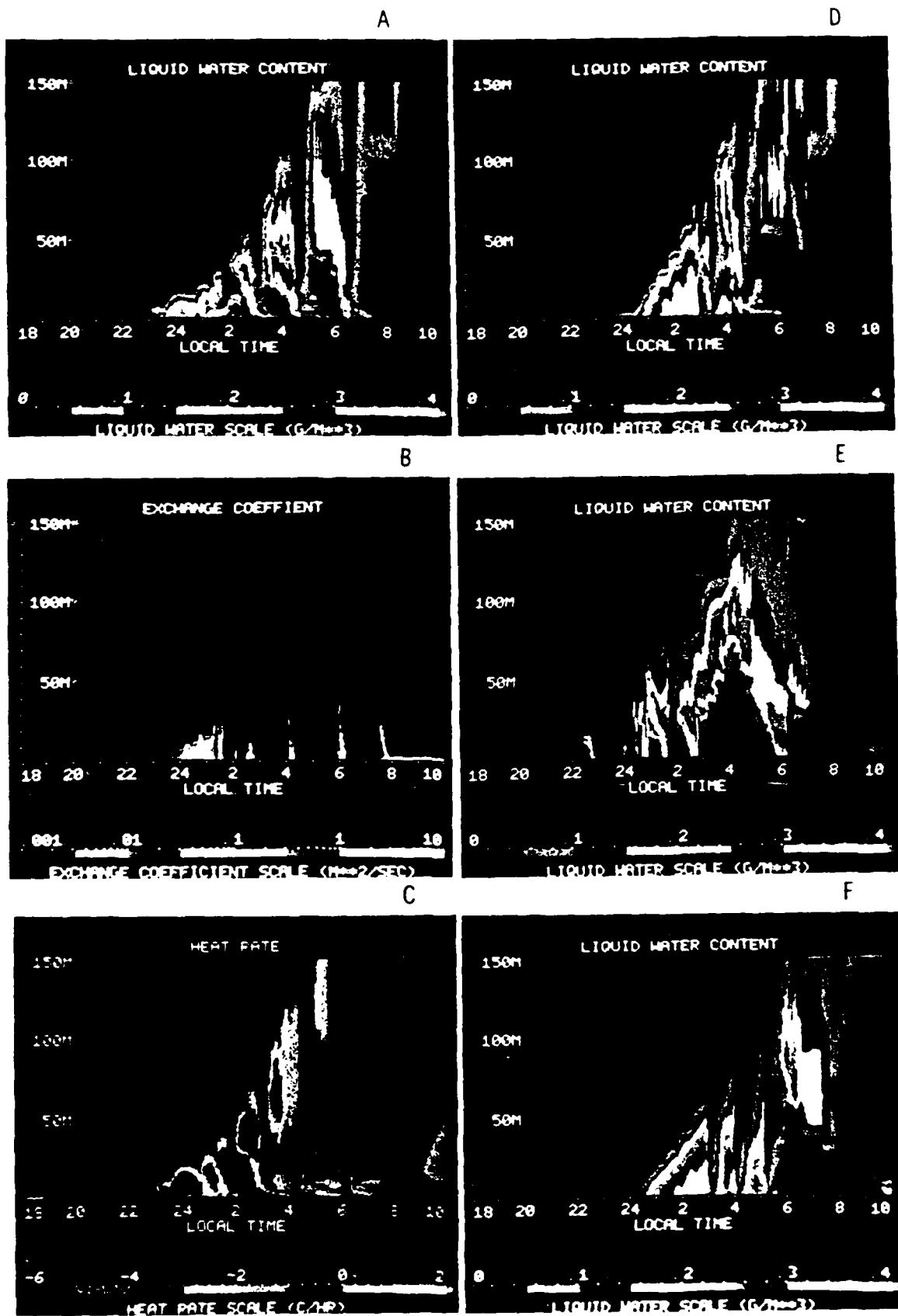In two cases, using the Blackadar (1979) and the Panofsky and Dutton (1984) eddy exchange methods,

FIG. 5. (a) Liquid water content. (b) eddy exchange coefficient. and (c) heating/cooling rate as a function of height and local time using the Blackadar (1979) turbulence formulation. Liquid water content for the following turbulence formulations. (d) Brost and Wyngaard (1978), (e) Panofsky and Dutton (1984), and (f) Shir (1973).

fog forms aloft at a height of 10–15 m and then lowers to the surface. In both cases, the fog formation aloft is associated with strong cooling rates at these levels in the absence of turbulent mixing. Additional case studies are needed to determine the conditions under which fog formation aloft, rather than at the surface, is likely.

During the initial fog development stage, atmospheric stability decreases. The surface loss of energy by radiation continues to decrease as the water column continues to increase. The result is an increasingly isothermal temperature structure near the ground and a steadily decreasing Richardson number. The initial fog growth stage is terminated by an abrupt suppression of turbulence generation due to a sharp increase in the Richardson number as a surface inversion becomes reestablished. Larger decreases in liquid water content result near the surface. In some cases, the liquid water seems to be "pumped" aloft, but, in most cases, the mixing of dry air from aloft depletes liquid water throughout all levels of the fog. There is a sharp decrease in value of the integrated water column and a corresponding increase in the surface radiation flux.

Each of these case studies predicts a series of fog dissipation and redevelopment episodes during the mature fog stage. These episodes, predicted to reoccur every 1–2 hours, are at least qualitatively similar to the near-surface liquid water measurements shown in Fig. 4. The models suggest that liquid water is generated in the upper regions of the fog by radiative cooling. Periods of increased turbulence generation due to destabilization of the boundary layer mix the liquid water from aloft to the surface.

In the case of strong and prolonged turbulence generation from 0300 to 0400 as predicted in the Panofsky and Dutton formulation, the fog lifts completely off the ground to become low stratus. Only with gradual decrease in strength of the turbulence generation does this low cloud lower to the surface.

In each of these four case studies, fog is completely dissipated after sunrise. In most cases, a low-level stratus forms with a base height at 100–200 m. However, evaporation of dew and soil moisture after sunrise causes a reformation of a shallow ground fog of height 5–10. Liquid water content in this shallow fog is predicted to be on the order of $w_l = 0.05$ g m^{-3} in most cases, but reaches 0.20 g m^{-3} for the Shir exchange method. This sunrise stage of fog thickening and reformation is reported by Jiusto and Lala. Final dissipation occurs at about 1030 in all cases.

5. Conclusions

Fog development is shown to be very sensitive to the formulation of turbulence generation. However, the simulations show the same stages of fog development as observed by Jiusto and Lala (1983a). These stages are defined as follows.

a. Sundown stage

The surface layer changes from lapse conditions to a strong surface inversion over a period of about two hours. Turbulence generation is suppressed. However, the predicted decrease in predicted surface temperatures is about half the rate observed. This suggests that the assumed initial conditions are incorrect. The replacement of the initial temperature profile by lapse conditions, the decrease of the initial relative humidity, and the decrease of the initial soil temperature gradient would all contribute to greater surface cooling.

b. Conditioning and fog formation stage

Surface cooling decreases at about 1°C h^{-1} and remains at this rate for several hours. Heat is transported downward to the surface by weak turbulence, and then is radiated away to space. Relative humidity increases in the lower 5–20 m to near saturated conditions. A very weak ground fog in the lower 1–5 m occasionally develops in this period. However, fog development is directly coupled with the destabilization of the lower atmosphere and with increases in turbulent mixing. These results are in agreement with the observations of Lala et al. (1982), which suggest that increased turbulence contributes to fog formation. They are not in agreement with the observations of Roach et al. (1976), which suggest that fog forms during lulls in turbulence generation.

Increased turbulent mixing rapidly lifts the surface inversion. Fog top height is directly correlated to the height of this inversion. Fog intensity (liquid water content) also is directly correlated to the strength of the turbulence. The region of maximum cooling lifts off the ground and becomes located in the upper third of the fog. Temperature, liquid water, visibility, heat and moisture fluxes, and cooling rate all show rapid variation during this period, especially in the upper regions of the fog.

c. Mature stage

The dense fog stage shows a series of fog development and dissipation episodes. The period of these episodes varies greatly with turbulence formulation. The Businger and Arya (1974) exchange formulation predicts a series of episodes with a periodicity of 40–60 min. However, Blackadar's (1979) exchange formulation predicts a series of fog episodes at the surface with a periodicity of about 1–2 h. This periodicity is in at least qualitative agreement with observations (Fig. 4). This model predicts that liquid water intensifies in the upper regions of the fog due to radiative cooling. It is only during periods of atmospheric destabilization that increased turbulence mixes this upper level liquid to the surface.
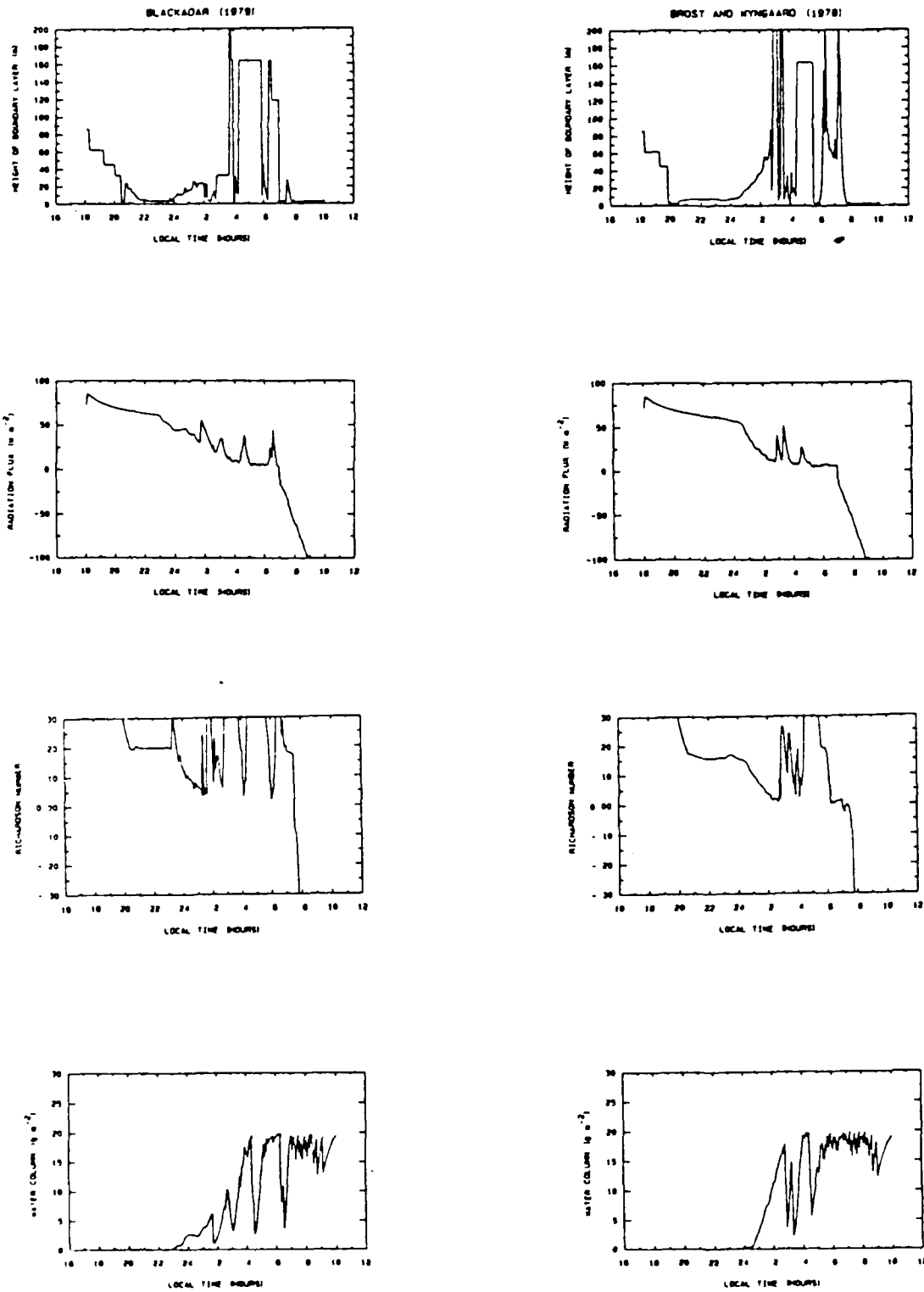
0016

FIG. 6. Height of the boundary layer, *h*; radiation flux at the surface; Richardson number, Ri; and water column as a function of height and local time using four turbulence formulations.
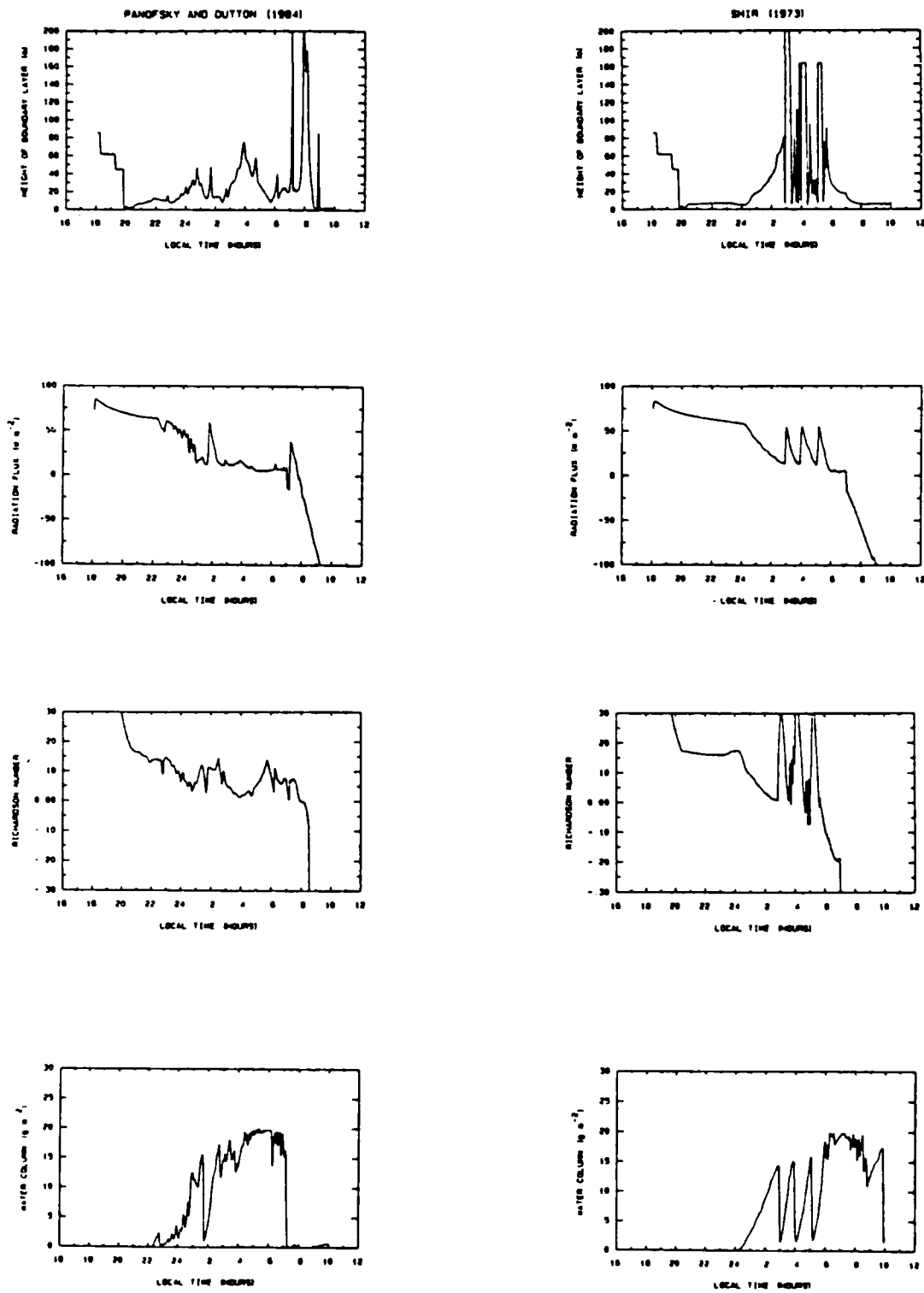
PANOFSKY AND DUTTON (1984)

SHIR (1973)

FIG. 6. (*Continued*)

d. Dissipation stage

Observations suggest that fog often intensifies after sunrise. The model results suggest that this is caused by increased turbulence generation mixing upper-level liquid to the surface. However, the models often predict the formation of a low-level stratus deck that prevents this intensification stage. Evaporation of dew and soil moisture supplies sufficient moisture to the atmosphere either to sustain the fog or to cause reformation of the fog. Final "burn-off" typically occurs between 1000 and 1100.

The various first-order closure turbulence models are based upon formulations that are based only upon simple gradients. Therefore, it is surprising to find qualitative agreement with observations to be relatively good. The various models predict quasi-periodic oscillations and longer-term fog dissipation and redevelopment episodes. However, the numerical simulation gives no hint of very short-period oscillations ($\sim$70 s) observed by Choularton et al. (1981), which may be associated with convective motions in the form of Benard cells.

These results are encouraging because they indicate that at least qualitative prediction of fog events may be feasible using relatively primitive formulations of turbulence generation. Nevertheless, it is possible that the similarities between the numerical model and the Jiusto and Lala observations are fortuitous. For instance, variation of geostrophic wind from 2 to 3 m s^{-1} may have a strong influence on the results. In order to improve and to verify the various models, a number of thorough case studies is required. It is important to have a detailed set of initial conditions and to know the vertical distribution of turbulent mixing, liquid water, heat fluxes, and moisture fluxes during these various fog development stages. Extension of the measurements to heights greater than the 16 meters currently available on the Albany tower would be most desirable. The model results show that much of the interesting fog development occurs in the 20–50 m level.

Andre, J. C., and L. Mahrt, 1982: The nocturnal surface inversion and influence of clear-air radiative cooling. *J. Atmos. Sci.*, **39**, 864–878.

Arya, S. P. S., 1981: Parameterizing the height of the stable atmospheric boundary layer. *J. Appl. Meteor.*, **20**, 1192–1202.

Baver, L. D., W. H. Gardner and W. R. Gardner, 1972: *Soil Physics.* 4th ed., Wiley and Sons, 498 pp.

Blackadar, A. K., 1962: The vertical distribution of wind and turbulent exchange in a neutral atmosphere. *J. Geophys. Res.*, **67**, 3095–3102.

——, 1979: High resolution models of the planetary boundary layer. *Adv. Environ. Sci. and Engineering, Vol. 1,* No. 1, X. Pfafflin and X. Ziegler, Eds., Gordon and Breach, 50–85.

Brost, R. A., and J. C. Wyngaard, 1978: A model study of the stably stratified planetary boundary layer. *J. Atmos. Sci.*, **35**, 1427–1440.

Brown, R., 1980: A numerical study of radiation fog with an explicit formulation of the microphysics. *Quart. J. Roy. Meteor. Soc.*, **106**, 781–802.

——, and W. T. Roach, 1976: The physics of radiation fog. II—A numerical study. *Quart. J. Roy. Meteor. Soc.*, **102**, 335–354.

Businger, J. A., 1966: Transfer of heat and momentum in the atmospheric layer. Prog. Arct. Heat Budget and Atmospheric Circulation, Santa Monica, Rand Corporation, 305–322.

——, and S. P. S. Arya, 1974: Height of the mixed layer in a stably stratified planetary boundary layer. *Advances in Geophysics,* Vol. 18A, Academic Press, 73–92.

——, J. C. Wyngaard, Y. Izumi and E. F. Bradley, 1971: Flux profile relationships in the atmospheric surface layer. *J. Atmos. Sci.*, **28**, 181–189.

Carl, D. M., T. C. Tarbell and H. A. Panofsky, 1973: Profiles of wind and temperature from towers over homogeneous terrain. *J. Atmos. Sci.*, **30**, 788–794.

Choularton, T. W., G. Fullarton, J. Latham, C. S. Mill, M. H. Smith and J. M. Stromberg, 1981: A field study of radiation fog in Meppen, West Germany. *Quart. J. Roy. Meteor. Soc.*, **107**, 381–394.

Delage, Y., 1974: A numerical study of the nocturnal atmospheric boundary layer. *Quart. J. Roy. Meteor. Soc.*, **100**, 351–364.

Dudis, J. J., 1972: The stability of a saturated, stably-stratified shear layer. *J. Atmos. Sci.*, **29**, 774–778.

Durran, D. R., and J. B. Klemp, 1982: On the effects of moisture on the Brunt-Väisälä frequency. *J. Atmos. Sci.*, **39**, 2151–2158.

Dyer, A. J., and E. F. Bradley, 1982: An alternative analysis of flux-gradient relationships at the 1976 ITCE. *Bound. Layer Meteor.*, **22**, 1–19.

Emmons, G., and R. B. Montgomery, 1947: Note on the physics of fog formation. *J. Meteor.*, **4**, 206–209.

Finnigan, J. J., and F. Einaudi, 1981: The interaction between an internal gravity wave and the planetary boundary layer. Parts I and II. *Quart. J. Roy. Meteor. Soc.*, **107**, 793–832.

Fleagle, R. G., 1953: A theory on fog formation. *J. Mar. Res.*, **12**, 43–50.

Forkel, R., W. G. Panhaus, R. Welch and W. Zdunkowski, 1984: A one-dimensional numerical study to simulate the influence of soil moisture, pollution and vertical exchange on the evolution of radiation fog. *Contrib. Atmos. Phys.*, **57**, 72–91.

Fraser, A. R., R. C. Easter and P. V. Hobbs, 1973: A theoretical study of the flow of air and fallout of solid precipitation over mountainous terrain. Part I. Airflow model. *J. Atmos. Sci.*, **30**, 801–812.

Gerber, H. E., 1981: Microstructure of a radiation fog. *J. Atmos. Sci.*, **38**, 454–458.

Hanel, G., 1976: The properties of atmospheric aerosol particles as functions of relative humidity at thermodynamic equilibrium with the surrounding moist air. *Adv. Geophys.*, **19**, 74–188.

Hillel, D., and C. H. M. van Bavel, 1976: Simulation of profile water

storage as related to soil hydraulic properties. *Soil Sci. Soc. Am. J.*, **40**, 797–815.

Jiusto, J. E., and G. G. Lala, 1982: Liquid water content in radiation fogs. *Preprints Conf. Cloud Physics*, Chicago, Amer. Meteor. Soc., 300–302.

——, and ——, 1983a: The fog project—1982. *Preprints Ninth Conf. Aerospace and Aeronautical Meteorology*, Omaha, Amer. Meteor. Soc., XXX–XXX.

——, and ——, 1983b: Cold environment fogs and measurements. *Int. Soc. Opt. Eng. Symp.*, Arlington, XX–XX.

Kondo, J., O. Kanechika and N. Yosuda, 1978: Heat and momentum transfers under strong stability in the atmospheric surface layer. *J. Atmos. Sci.*, **35**, 1012–1021.

Lala, G. G., M. B. Meyer and J. E. Jiusto, 1978: Cloud physics and boundary layer measurements in radiation fog. *Preprints Conf. Cloud Physics and Atmospheric Electricity*, Issaquah, Amer. Meteor. Soc., XX–XX.

——, J. E. Jiusto, M. B. Meyer and M. Kornfield, 1982: Mechanisms of radiation fog formation on four consecutive nights. *Preprints Conf. Cloud Physics*, Chicago, Amer. Meteor. Soc., 9–11.

Lalas, D. P., and F. Einaudi, 1974: On the correct use of the wet adiabatic lapse rate in stability criteria of a saturated atmosphere. *J. Appl. Meteor.*, **13**, 318–324.

Mason, J., 1982: The physics of radiation fog. *J. Meteor. Soc. Japan*, **60**, 486–498.

McDonald, J. E., 1963: The saturation adjustment in numerical modeling of fog. *J. Atmos. Sci.*, **20**, 476–478.

Monteith, J. L., 1957: Dew. *Quart. J. Roy. Meteor. Soc.*, **83**, 322–341.

Neiburger, M., and W. Chien, 1960: Computations of the growth of cloud drops by condensation using an electronic digital computer. *Physics of Precipitation*, H. Werkmann, Ed., Publisher, 191–210.

Nieuwstadt, F. T. M., 1984: The turbulent structure of the stable, nocturnal boundary layer. *J. Atmos. Sci.*, **41**, 2202–2216.

Pandolfo, J. P., 1966: Wind and temperature for constant flux boundary layers in lapse conditions with a variable eddy conductivity to eddy viscosity ratio. *J. Atmos. Sci.*, **23**, 495–502.

Panofsky, H. A., and J. A. Dutton, 1984: *Atmospheric Turbulence.* Wiley and Sons, 397 pp.

Roach, W. T., 1976: On the effect of radiative exchange on the growth by condensation of a cloud or fog droplet. *Quart. J. Roy. Meteor. Soc.*, **102**, 361–372.

——, R. Brown, S. J. Caughey, J. A. Garland and C. J. Readings, 1976: The physics of radiation fog. Part I: A field study. *Quart. J. Roy. Meteor. Soc.*, **102**, 313–333.

Rodhe, B., 1962: The effect of turbulence on fog formation. *Tellus*, **14**, 49–86.

Shir, C. C., 1973: A preliminary numerical study of atmospheric turbulent flows in the idealized planetary boundary layer. *J. Atmos. Sci.*, **30**, 1327–1339.

Sievers, U., R. Forkel and W. Zdunkowski, 1983: Transport equations for heat and moisture in the soil and their application to boundary layer problems. *Contrib. Atmos. Phys.*, **56**, 58–83.

Taylor, G. I., 1917: The formation of fog and mist. *Quart. J. Roy. Meteor. Soc.*, **43**, 241–268.

Welch, R. M., and B. A. Wielicki, 1986: The stratocumulus nature of fog. *J. Climate Appl. Meteor.*, **42**, 101–111.

Wyngaard, J. C., 1975: Modeling the planetary boundary layer—extension to the stable case. *Bound. Layer Meteor.*, **9**, 441–460.

Xing-Sheng, L., J. E. Gaynor and J. C. Kaimal, 1983: A study of multiple stable layers in the nocturnal lower atmosphere. *Bound. Layer Meteor.*, **26**, 157–168.

Zdunkowski, W. G., R. M. Welch and J. Paegle, 1976: One-dimensional numerical simulation of the effects of air pollution on the planetary boundary layer. *J. Atmos. Sci.*, **33**, 2399–2414.

——, W. G. Panhaus, R. M. Welch and G. N. Korb, 1982: A radiation scheme for circulation and climate models. *Contrib. Atmos. Phys.*, **55**, 215–237.

Zhang, D., and R. A. Anthes, 1982: A high-resolution model of the planetary boundary layer—sensitivity tests and comparisons with SESAME-79 data. *J. Appl. Meteor.*, **21**, 1594–1609.

Zilitenkevich, S. S., 1972: On the determination of the height of the Ekman boundary layer. *Bound. Layer Meteor.*, **3**, 141–145.

——, 1975: Resistance laws and prediction equations for the depth of the planetary boundary layer. *J. Atmos. Sci.*, **32**, 741–752.

The Stratocumulus Nature of Fog

RONALD M. WELCH

Institute of Atmospheric Sciences, South Dakota School of Mines and Technology, Rapid City, SD 57701

BRUCE A. WIELICKI

Atmospheric Sciences Division, NASA/Langley Research Center, Hampton, VA 23665

ABSTRACT

Landsat Multispectral Scanner (MSS) and Thematic Mapper (TM) digital data are used to remotely sense fog properties. These include fog cell size distribution, cell aspect ratio (the ratio of the length of the major and minor axes of the cells), and cell orientation angle. The analysis is carried out for four fog scenes, three high-inversion radiation fogs in central California, and one advection fog in eastern South Dakota.

Results for these initial fog studies indicate that 1) fogs are stratocumulus in nature, being composed of individual cellular structures; 2) the reflectance properties vary strongly across the cells, suggesting considerable variation in liquid water content; 3) fogs often are patchy, often revealing surface features between fog cells; 4) the ratio of wavelength (λ) between cells and the height of the boundary layer (h) is $\lambda/h \approx 2-3$, in agreement with values obtained for Benard cells and longitudinal rolls observed in cloud systems; 5) the typical horizontal aspect ratio of fog cells is about a factor of 2; and 6) observed quasi-periodic oscillations of measured fog variables may be caused by advection of the cellular structures across the observational site.

1. Introduction

Fogs often form almost simultaneously over large areas of hundreds of square kilometers. Observation programs using towers and balloons (Pilie *et al.*, 1975; Roach *et al.*, 1976; Lala *et al.*, 1982; Gerber, 1981) show that fogs are not uniform, but rather have high frequency variations in most measured variables.

Roach (1976) was the first to observe that fogs often have quasi-periodic oscillations in the measured properties such as temperature, liquid water, visibility, wind speed, radiation and turbulence generation. Gerber (1981) and Lala *et al.* (1982) also reported similar occurrences of quasi-periodic oscillations. The reported periods of oscillation range from 10–30 min, with most observations in the range of 15–20 min. Lala *et al.* (1982) suggested that nights with stronger atmospheric stability have lighter winds, shorter periods of oscillation, and greater likelihood of patchy fog.

Gerber (1981) found that dense fog was composed of highly structured and sharply defined local regions. Roach *et al.* (1976) suggested that variations in the nature and slope of local terrain are at least partially responsible for the observed local structure. Roach (1976) attributes the quasi-periodic oscillations to gravity waves propagating at the top of the boundary layer. He also suggested that variations caused by advection are on the order of 5–10 min, while the longer quasi-periodic oscillations may be controlled by a fluctuating balance between radiation cooling at fog top

and turbulence generation. Welch and Ravichandran (1985) came to a similar conclusion, with destabilization of the boundary layer producing brief periods of strong turbulent mixing. However, the model generally predicts oscillations on the order of 40–60 min, considerably longer than the observations.

The present study focuses upon fog spatial structure observed using extremely high spatial resolution Landsat Multispectral Scanner (MSS) and Thematic Mapper (TM) digital data. It is shown that fogs, at the time of the Landsat overpasses, are composed of cellular elements. That GOES and AVHRR satellite imagery has shown little hint of this cellular structure is due to the fact that the fog elements are generally smaller than the spatial resolution available on these satellite platforms.

2. Landsat satellite data

Landsat satellites provide extremely high spatial-resolution data in several spectral bands. The Multispectral Scanner (MSS) instrument has a nominal-spatial resolution of 57 meters with four narrow spectral bands centered at 0.55, 0.65, 0.75, and 0.95 μm wavelengths. The Thematic Mapper (TM) instrument has six shortwave and near-infrared spectral bands centered at 0.48, 0.56, 0.66, 0.83, 1.65, and 2.21 μm with a nominal spatial resolution of 28.5 meters. The TM also has an 11.5 μm spectral band with 114 meter spatial
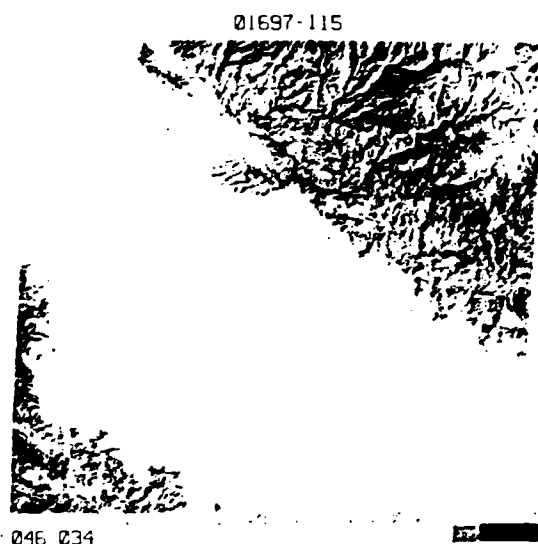
FIG. 1. Landsat MSS image of high-inversion fog near Merced. CA, at 1759 GMT 6 January 1981; spatial resolution is 57 m.

FIG. 3. Landsat MSS image of advection fog near Sioux Falls. SD. at 1640 GMT 7 November 1983; spatial resolution is 57 m.

resolution. The Landsat satellites are in Sun-synchronous orbits, sampling the Earth at approximately 0930 and 2130 local time. The satellite obtains data for a 180-km wide north–south strip along the ground-track. This strip is then broken up into 170-km × 180-km scenes. Landsat data provides the spatial resolution needed to accurately define the extent of the fog episode and spatial variability within the fog.

Figure 1 shows a fog episode in the California Inland Valley, centered near the City of Merced, at 1759 GMT 6 January 1981. The image is for channel 7 (0.8–1.1

FIG. 2. GOES image of fog in the California Inland Valley at 1746 GMT 6 January 1981; spatial resolution is 1 km.

μm). A section of the Sierra Nevada Mountains is visible in the upper right-hand corner. The 57-meter spatial resolution on this MSS image is sufficient to show that the fog has considerable structure. However, the gray-scale used to process this image has been chosen to enhance surface features at the expense of fog features. This is an example of high-inversion wintertime radiation fogs which form when polar maritime air stagnates under a persistent high pressure system (Taylor, 1941; Holets and Swanson, 1981).

Figure 2 shows a corresponding GOES satellite image taken at 1746 GMT. The spatial resolution is 2 km, with no hint that the fog is composed of small cellular structures. The Landsat scene shown in Fig. 1 corresponds to a 180 × 170 km section outlined approximately by the black box in Fig. 2.

A second Landsat MSS image is shown in Fig. 3. This is an advection fog covering eastern South Dakota and Nebraska at 1640 GMT 7 November 1983. Sioux Falls, South Dakota, in the upper right-hand corner of the image, reported fog with visibility of two miles at the time of the Landsat overpass, and a maximum surface wind speed of 14 knots from the south at 180°. The body of water is the Gavins Point Reservoir on the Missouri River. This fog event was very widespread, with Dodge City, Kansas, reporting one-quarter mile visibility and Abilene, Texas, reporting two-mile visibility.

Figure 4 shows two Landsat TM scenes of the San Francisco Bay region. Figure 4a shows channel 4 (0.76–0.90 μm) at 1814 GMT 31 December 1982, and Fig. 4b shows channel 4 at 1815 GMT 1 February 1983. Both cases show the western extremity of fog events covering the California Inland Valley.
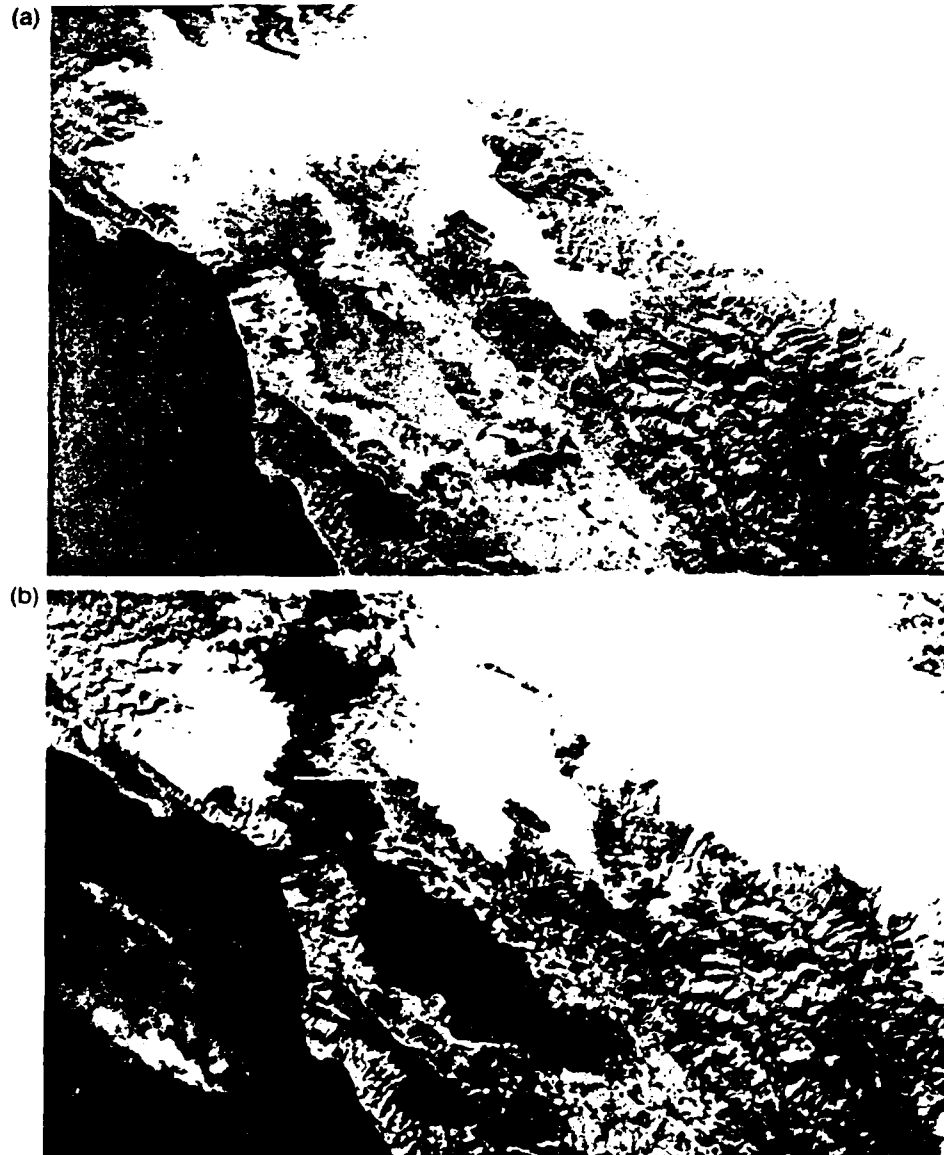
FIG. 4. Landsat TM images of the San Francisco Bay region at (a) 1814 GMT 31 December 1982;
and (b) 1815 GMT 1 February 1983. Spatial resolution is 28.5 m.

3. Image processing of the fog scenes

For each of the fog scenes, digital count is converted to nadir reflectance using the calibration coefficients given by Robinove (1982) for MSS channel 3 data and by Castle et al. (1984) for the TM channel 4 data. Castle et al. estimate a calibration accuracy of 5%. Figure 5(a–c) gives series of false color subsections of the fog event shown in Fig. 1. The color scale ranges from black at zero counts to white at 97 counts. One color is assigned to each digital count value, and the discrete color scale

is shown at the top of the image. The scale represents a linear range in pixel reflectance from 3% to 95%.

Figure 5a shows a 2048 × 2048 pixel subsection of the fog, corresponding to 116 km on a side. The false color processing brings out the graininess of the fog. The lower right-hand side of the image (red) is a region of maximum reflectance, indicating that the fog in this region is optically more dense. This may be caused by thicker fog in this region, or fog with larger liquid water contents, or by the combination. The fog appears to be less intense in the upper left-hand side of the image
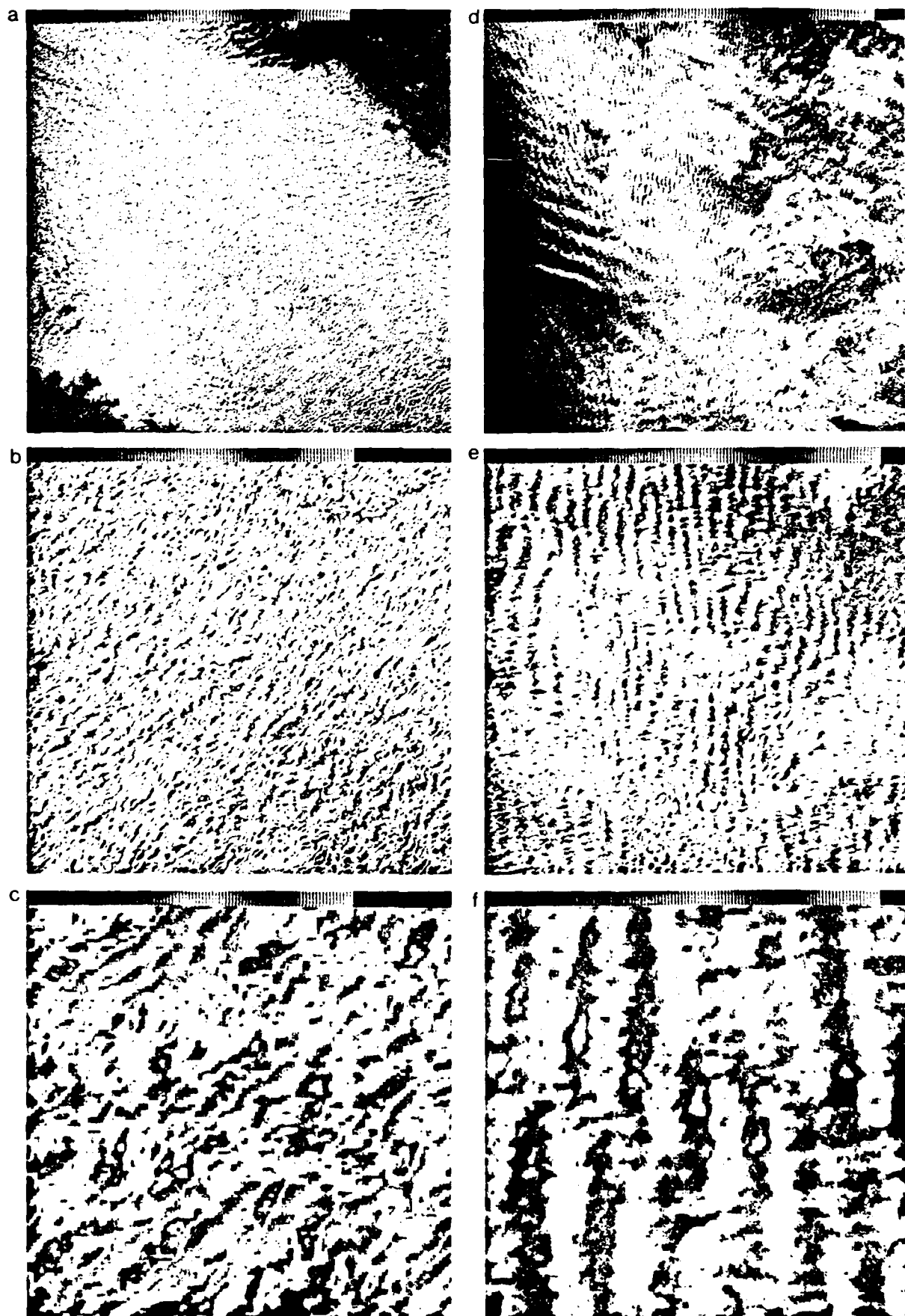
Fig. 5. False color images of fog regions. Figures 5a–c correspond to Fig. 4 and Figs. 5d–f correspond to Fig. 3. Figures 5a and 5d show 116 × 116 km regions (2048 × 2048 pixels) of the fogs. Figs. 5b and 5e show 30 × 30 km regions, and Figs. 5c and 5f show 8 × 8 km regions, respectively.
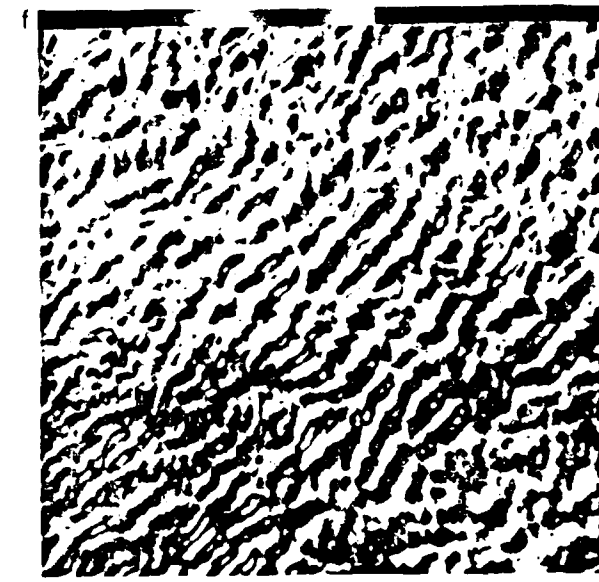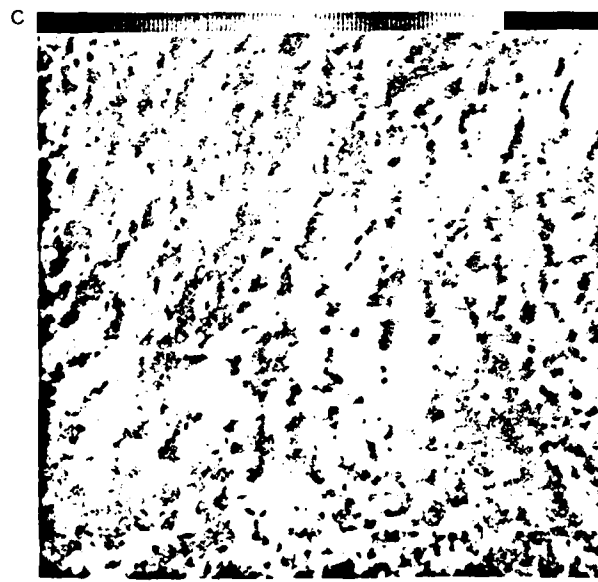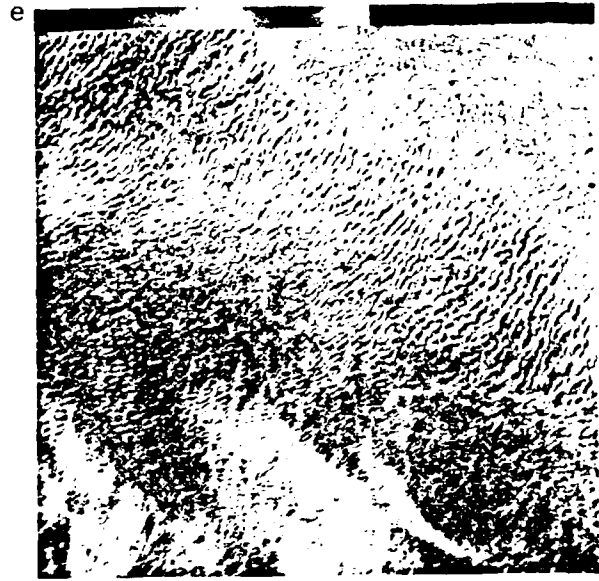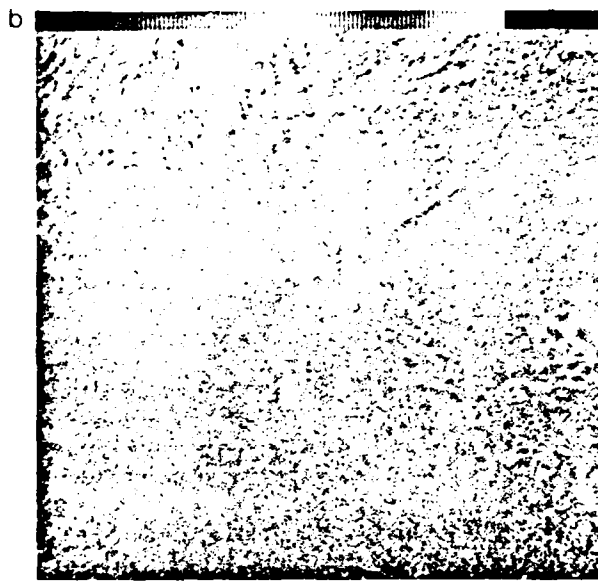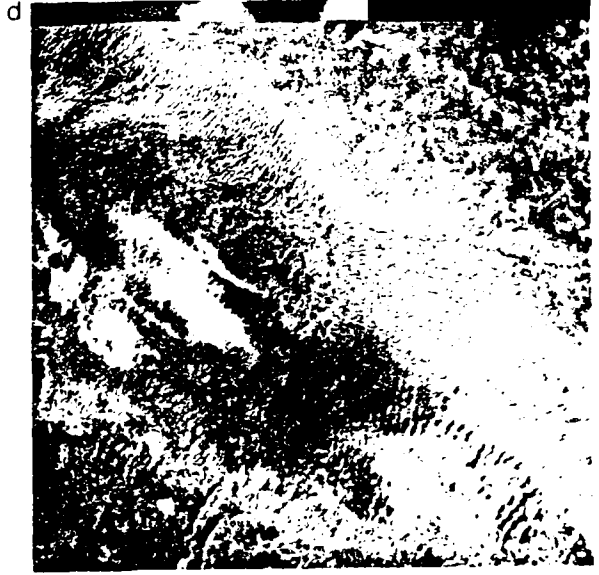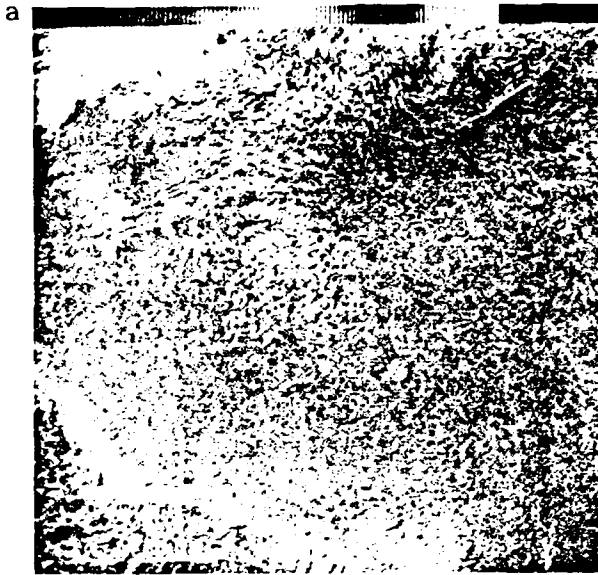
and around the edges of the fog. In these regions one expects the highest rate of fog dissipation.

Figure 5b shows a 30 km subsection, taken to the right and below the center of Fig. 5a. The individual fog elements become visible in this image. Finally, Fig. 5c shows an 8 km subsection taken from the upper left-hand corner of Fig. 5b. The size of the individual fog elements now can be measured, along with their orientation. The blue regions represent clear or nearly-clear regions between the individual fog elements. The patchiness of the fog, as well as its stratocumulus nature, is evident in this image.

Figures 5(d–e) give a corresponding series of false color subsections of the advection fog shown in Fig. 3. The color scale ranges from 0 to 118 counts, representing a range in pixel reflectance from 3% to 105%. Figure 5d shows a 116 km section of this advection fog. The fog is composed of large patchy regions. Figure 5e is a 30 km subsection taken from the center of Fig. 5d, showing the fog elements which have the appearance of cloud streets. Figure 5f shows an 8 km subsection taken at the upper boundary just left of center of Fig. 5e. The individual fog streets appear to be about 0.75 km in width. The structure of this fog is similar to that observed in a fair weather cumulus cloud street discussed by Wielicki and Welch (1986). The spacing between cloud streets is on the order of 1.5 km for the fog, as compared to about 4 km for the cloud street case.

Figure 6 shows false color images of two San Francisco Bay area fogs (Fig. 4). Figures 6a and 6d show 60 km subsections; Figs. 6b and 6e show 30 km subregions; and Figs. 6c and 6f show 8 km subregions, respectively. The fog event on 31 December 1982 shown in Figs. 6(a–c) is the most uniform of the four fogs analyzed. The color scale ranges from 0 to 104 counts, representing a reflectance range from −1% to 62%. Variations in optical depth (i.e., reflectance) are small, with no patchy regions in which the ground is visible. An apparent rift in the fog is visible in the upper right-hand corner of Figs. 6a and 6b. The cause is not known, but may be associated with shifts in wind speed and direction due to surface topography.

Figure 6(d–f) shows a much more variable fog, with some highly reflecting regions in an irregular pattern. The image color scale ranges from 0 to 153 counts, representing a reflectance range of −1% to 79%. The cell structure shown in Fig. 6f is the smallest of the four cases studied. Cell width is on the order of 0.3 km with separations between cells on the order of 0.5–0.6 km.

4. Fog cell size distributions

For 57-m Landsat MSS resolution data, even a 0.25 km fog element will be composed of roughly 15 data pixels. For TM data, there will be about four times this number of pixels. In either case, there are sufficient data pixels to distinguish between fog edge pixels and fog interior pixels. Once the edge pixels are distinguished, the individual fog structures can be grouped into individual fog cells. Statistics then can be generated, grouped into fog cell size classes. A thorough examination of this method is given by Wielicki and Welch (1986).

The procedure is as follows. First, a fog threshold digital reflectance count, V_c, is set. Each pixel with a digital count greater than V_c is flagged as a fog pixel. Second, if a fog pixel has at least one of its sides adjacent to a clear pixel, then the pixel is flagged as an edge pixel. Third, fog edge and fog interior pixels are grouped into individual fog cells. A fog element is determined to be unique when it has no edge pixels adjacent to another fog cell.

The preceding analysis is accomplished in a single pass through the Landsat satellite data, starting at the top of the image and examining three scan lines at a time while moving from top to bottom through the image. An example of this process is given by Wielicki and Welch (1986). Fog cell area is determined as the number of fog pixels multiplied by the pixel area (57 × 57 m for MSS data and 28.5 × 28.5 m for TM data). Effective cell diameter is defined as a circle of area equal to the area of the fog element.

All fog cells in the image are grouped into a finite number of size classes by effective fog element diameter D. Because the number of fog elements tends to decrease exponentially with increasing fog cellular size, intervals are chosen in equal steps of 0.4055 in $\ln D$. For this step size, each fog size boundary increases by a factor of 1.5 (i.e., 0.059, 0.088, 0.132, 0.198, 0.296, 0.444, 0.667, 1.00 km, . . .). This selection of fog cell size classes maintains a large number of fog elements in each size class for statistical reliability.

Figure 7 shows the fog cellular size distribution for each of the four fog case studies. In order to best delineate cloud cellular structure within the cloud field, thresholds V_c were chosen so that one-half of the fog area was brighter than the threshold V_c. The analyzed area is the same 2048 × 2048 pixel area shown in Figs. 5a, 5d, 6a, and 6d. The fog cell size distribution is given as the number of fog elements per 1 km² surface area per 1 km fog cell diameter range. All four scenes give similar numbers of fog elements below 0.5 km in diameter. The South Dakota advection fog (Fig. 3) and the San Francisco Bay area fog (Fig. 4b) have the smallest number of fog cells in the intermediate size classes (0.5–2.5 km), while the patchy central valley fog (Fig. 1) has the largest number of cells in this size range. The more uniform fog (Fig. 4a) has no cell sizes greater than 14 km in effective diameter. In contrast,
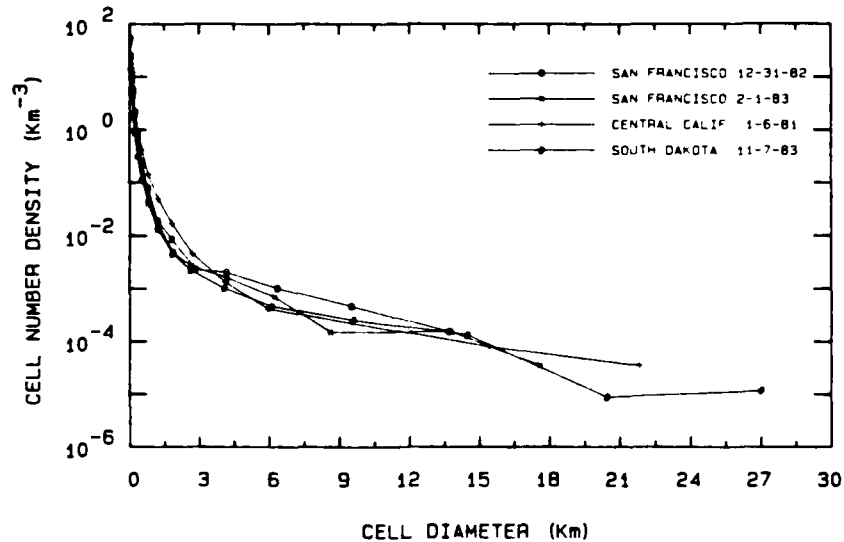
FIG. 7. Fog cell size distribution vs cell equivalent diameter for the four fog case studies.

the central California fog has cells as large as 22 km, and the advection fog cells are as large as 27 km. Nevertheless. Fig. 7 shows that the different fogs are surprisingly similar in the size distribution of the cell structures.

Figure 8a shows the fog cell horizontal aspect ratio as a function of cell size for all size classes containing four or more fog cells. Aspect ratio is defined as the ratio of the length of the major and minor axes for each cell. For a circular element, aspect ratio is unity. Figure 8a shows that the smallest cells have an average aspect ratio of two for all four case studies. The aspect ratio increases with increasing cell size, reaching a value of about ten for the largest cells. The standard deviation of aspect ratio within a fog cell size class is about one for the smallest clouds. The standard deviation increases to about six for cells with equivalent diameters of about 10 km. The advection fog (Fig. 3) and the San Francisco Bay area fog (Fig. 4b) show large mesoscale variability and have larger standard deviations of aspect ratio. Nevertheless, there is a clear trend towards larger aspect ratios for the larger cells for all four fog cases. Note that aspect ratios shown are for fog cells with diameters greater than twice the Landsat pixel resolution.

Figure 8b shows the orientation angle of the cells as a function of cell size. The orientation angle is defined as 0° for elements aligned vertically in the image, increasing clockwise. The Landsat image is aligned at about 10° from north; therefore 10° should be added to each value shown in Fig. 8b to convert to earth ref-

erence. The smaller elements of the fogs are aligned in a NE–SW orientation at about 40° from north. Figures 5c and 6f show this orientation. On the other hand, the advection fog has orientation angles (Fig. 8b) of about 20° from north for cells with equivalent diameters of 0.5–2 km. Cells of this size range are conspicuous in Fig. 5f, and are aligned in a more nearly N–S orientation than are the smaller cells. Note that the largest cells in each fog tend to prefer a more E–W orientation. The fogs in Figs. 3 and 4a gave large standard deviations of fog cell orientation angle, presumably due to the mesoscale variability seen in Fig. 3 and the lack of well-defined fog streets in Fig. 4a.

5. Discussion

A number of investigations during the last five decades have focused upon the generation of Benard cells and longitudinal rolls (Ackerman, 1967; Kamiko and Okano, 1971; Kuettner, 1971; Agee et al., 1973; Krishnamurti, 1975; LeMone, 1976; Agee and Lomax, 1978; Brown, 1980; Agee, 1984; Atkinson, 1981). If wind direction and wind speed vary slowly with height, then Vinnichenko et al. (1973) point out that two-dimensional cells typically are formed with longitudinal bands elongated along the wind direction.

Wind direction at Sioux Falls, South Dakota, on 7 November 1983 was reported to be 170° near the surface. Due to surface friction, one expects a veering of the wind of 50°–60° under stable conditions. Such values, when added to the reported value of 170°, give
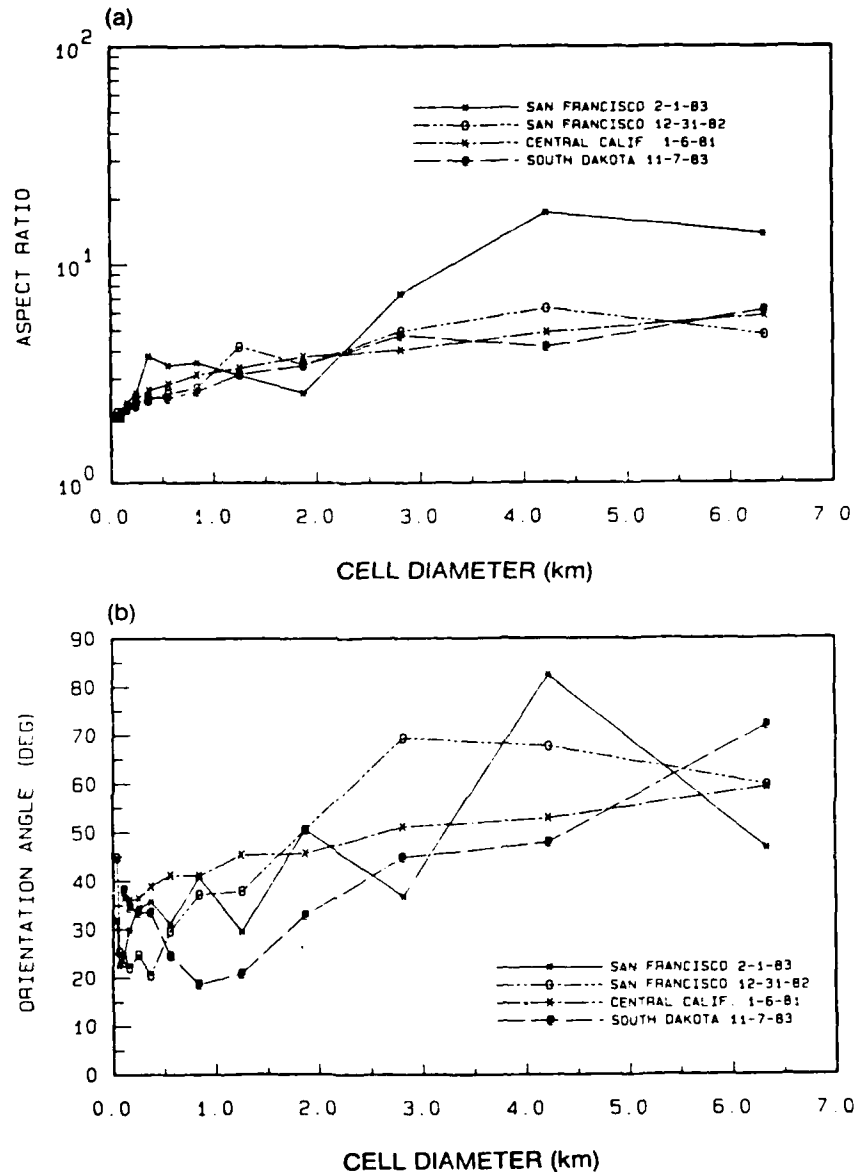
FIG. 8. (a) Fog cell aspect ratio vs cell equivalent diameter, and (b) cell orientation angle
with respect to the top of the image vs cell equivalent diameter.

wind directions aloft of 220°–230°. Assuming that the
fog elements align along the wind direction, values of
220°–230° are consistent with the statistical evaluation
shown in Fig. 8b. Wind speeds have not been evaluated
for the California fogs.

A number of investigators have studied the relation-
ship of cloud element size and the height of the bound-
ary layer. Applying linear stability analysis, Pellew and
Southwell (1940) found that circular cells were char-
acterized by $D = 2.16\,h$, where D is the cell diameter
and h is the height of the boundary layer. Walter and
Overland (1984) observed fog longitudinal rolls from
satellite imagery. They delineated a hierarchy of wave-

length (λ) scales of organized circulations, with λ
$= 0.3$–0.5 km due to the turbulent plumes and 1.3–
1.7 km due to inflection point instability (Brown, 1972,
1980). Theoretical studies suggest the ratio λ/h in the
range of 1.5–4 (Kelley, 1983).

Under stable conditions such as found in fog epi-
sodes, h is the inversion height. Holets and Swanson
(1981) report observations made in the high-inversion
fog episodes of the California central valley. They report
maximum fog layer heights of about 500 m and min-
imum heights of about 200 m. Therefore a value of
300 m for h during the time of the Landsat overpasses
seems reasonable. Typical wavelengths in the four fog

cases range from $\lambda = 0.5$–0.6 km for the "uniform" fog case (Fig. 6a–c) to $\lambda \approx 1$ km for the other fogs. Therefore we estimate that values of $\lambda/h = 2$–3 are representative of the present fog cases. Since these values are consistent with values found by Kelley (1983), we are led to the hypothesis that processes occurring in fogs are similar, but on a smaller scale, to those processes responsible for Benard cloud cells, longitudinal rolls, topographically induced gravity waves, and cloud top entrainment instability.

Once the height of the boundary layer is known, a first-order estimate of the vertical profile of the turbulent exchange coefficient (K) can be made (Brost and Wyngaard, 1978),

$$K = ku_*z(1 - z/h)^{1.5}/\phi \quad \text{for} \quad x \leqslant h \quad (1)$$

where k is von Karman's constant ($k = 0.4$) and u_* is the friction velocity. Holets and Swanson (1981) report wind speeds typically on the order of 2 m s^{-1} at a height of 10 m. A representative value for the friction velocity is estimated to be $u_* \approx 0.1$ m s^{-1} and the value of h is taken to be 300 m. Function ϕ is a stability correction factor which is usually parameterized in terms of the Richardson number (Ri) or the Obukhov height.

On the basis of fog modeling, a value of Ri ≈ 0.1 is adopted representing the fact that the high inversion fogs exist under conditions of strong inversions. For such stable conditions

$$\phi \approx 1 + 5\text{Ri}, \quad (2)$$

or $\phi \approx 1.5$. For these values, Eq. (1) suggests maximum turbulent mixing coefficients on the order of 1 m^2 s^{-1}. Such values are consistent with model predictions (Forkel et al., 1984; Welch and Ravichandran, 1985) during the morning hours after sunrise, suggesting relatively isothermal vertical profiles and uniform liquid water vertical profiles at least in the lower 100 m of the fog. At present, these conclusions cannot be verified, as field programs have not emphasized turbulence measurements in fogs. These large eddy diffusion rates also suggest that mixing with the drier environmental air surrounding the fog may be an important process for dissipation. Solar radiation heats the surrounding surfaces, causing a circulation pattern to be set up analogous to a land–sea breeze (Gustafson and Wasserman, 1976). Time lapse satellite images confirm that fogs tend to dissipate from the edges inward (Gurka, 1978).

Landsat images of two fog events are shown in Fig. 9, shortly before dissipation. Figure 9a shows the Sacramento region on 4 March 1979 which had reported 0.25 mile visibility at 0700 local time; the airport reported 5 mile visibility in haze at the time of the Landsat overpass. Figure 9b shows the Merced region on 11 February 1981 with reported light fog at dawn; this is the same region as shown in Fig. 1. These are the final remnants of fog episodes which earlier covered the California Inland Valley. The cell size is large, indi-
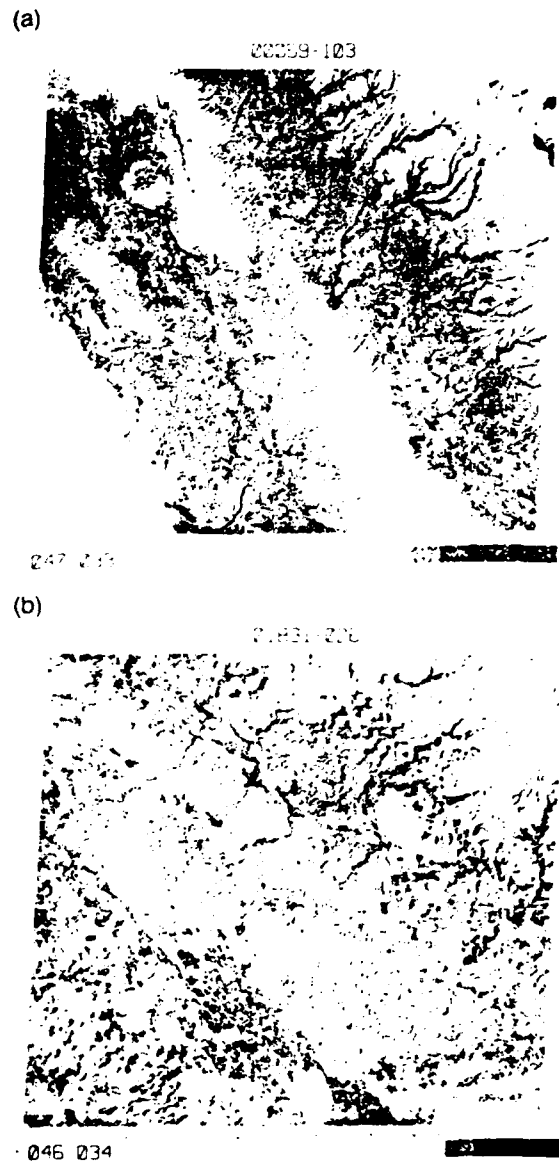
FIG. 9. Landsat MSS images of fog episodes showing dissipation remnants in the California Inland Valley (a) near Sacramento on 4 March 1979; and (b) near Merced on 11 February 1981.

cating large turbulent mixing ratios. This may be supplementary evidence supporting the hypothesis that the fog dissipates from its edges inward.

Finally, we consider the questions of the quasi-periodic oscillations observed in the measurements of Roach et al. (1976), Gerber (1981), and Lala et al. (1982). First, assume that the larger fog elements typically are separated by distances on the order of $\lambda \approx 1$ km, as seen in the Landsat images. Second, take the wind speed (u) as 2 m s^{-1}, a value typical of high pressure under which fog forms. The resulting time, $t = \lambda/v$, is 8–9 min, or about half the value reported for

the quasi-periodic oscillations (e.g., Roach, 1976). However, note that the wavelength λ is measured perpendicular to the wind speed, and that fog elements typically align along the wind direction. Since the typical aspect ratio for fog cellular elements is a value of 2, one would expect that the typical distance between cellular elements in the wind direction is about 2λ. The corresponding time is then $t = 2\lambda/v$, or 16–18 min. This value is in close agreement with the observed quasi-periodic oscillations of measured fog parameters. This suggests that the observed quasi-periodic oscillations may be a result of fog cells advected across the observational site.

6. Conclusions

The present results show that high resolution Landsat data is a valuable tool in the investigation of fog properties. The Landsat data provide information concerning regional fog coverage, the patchiness of fogs, cell size distribution, and cell aspect ratio and orientation angle. The major conclusions of this preliminary study are

1) For the four case studies, Landsat imagery shows fogs to be composed of individual cellular elements and to have an appearance similar to stratocumulus fields.

2) Most cellular fog elements show considerable variation in reflectance properties (i.e., optical depth) due to variations in liquid water content and/or fog thickness. However, infrared TM images do not show much grainy texture, indicating that fog thickness is relatively constant. Therefore the variations of reflectance values must be primarily associated with variations in liquid water content. The patchy nature of fog is clearly evident in the image processed scenes.

3) The number of cells decreases exponentially with increasing cell diameter, a characteristic also observed in cumulus cloud studies (Plank, 1969; Wielicki and Welch, 1986). The size distribution is remarkably similar for both radiation fogs and advection fogs, with no clear differentiation between the two types. However, the advection fog shows a stronger tendency for the fog elements to form cloud streets.

4) The wavelength (λ) between the larger fog elements is on the order of 1 km for three of the case studies, but with values as low as 0.5 km for the more "uniform" fog case. Using a value of 300 m as an estimate for the height of the boundary layer in high inversion fogs (Holets and Swanson, 1981), we obtain the ratio $\lambda/h \approx 2$–3, in agreement with studies of cloud systems (Kelley, 1983). These results suggest that the processes responsible for Benard cells and longitudinal rolls observed in clouds probably are also responsible for such structure observed in the Landsat fog images. Close to the surface, friction limits the scale of turbulent mixing, thereby producing cellular elements of smaller size. Applying arguments for gravity waves to cellular convection (Vinnichenko et al., 1973), it appears that the shorter the wave (the distance between cellular elements), the less stable is that cellular element.

5) The results suggest for conditions typical of radiation fogs, that the quasi-periodic oscillations measured in fogs may be the result of fog cells advected across the observational site. The period of 16–18 min is in close agreement with the period of 15–20 min typically found in fogs. However, the present preliminary study includes only four fog case studies for only two different regions. Considerably more effort needs to be expended to determine how representative these results are for fogs in different regions. Landsat observations also are limited to overpasses in the morning hours. Nocturnal observations should be made to determine if the present results are representative of conditions before sunrise.

REFERENCES

Ackerman, B., 1967: The nature of the meteorological fluctuations in clouds. *J. Appl. Meteor.*, **6**, 61–71.

Agee, E. M., 1984: Observations from space and thermal convection: a historical perspective. *Bull. Amer. Meteor. Soc.*, **65**, 938–949.

——, T. S. Chen and K. E. Dowell, 1973: A review of mesoscale cellular convection. *Bull. Amer. Meteor. Soc.*, **54**, 1004–1012.

——, and F. E. Lomax, 1978: Structure of the mixed layer and inversion layer associated with patterns of mesoscale cellular convection during AMTEX 75. *J. Atmos. Sci.*, **35**, 2281–2301.

Atkinson, B. W., 1981: *Meso-Scale Atmospheric Circulations.* Academic Press, NY, 495 pp.

Brost, R. A., and J. C. Wyngaard, 1978: A model study of the stably stratified planetary boundary layer. *J. Atmos. Sci.*, **35**, 1427–1440.

Brown, R. A., 1972: On the inflection point instability of a stratified Ekman boundary layer. *J. Atmos. Sci.*, **29**, 850–859.

——, 1980: Longitudinal instabilities and secondary flows in the planetary boundary layer: a review. *Rev. Geophys. Space Phys.*, **18**, 683–697.

Castle, K. R., R. G. Holm, C. J. Kastner, J. M. Palmer, P. N. Slater, M. Dinguirrard, C. E. Ezra, R. D. Jackson and R. F. Savage, 1984: In flight absolute radiometric calibration of the thematic mapper. *IEEE Trans. Geo. Remote Sens.*, **22**, 251–255.

Forkel, R., W. G. Panhaus, R. Welch and W. Zdunkowski, 1984: A one-dimensional numerical study to simulate the influence of soil moisture, pollution and vertical exchange on the evolution of radiation fog. *Contrib. Atmos. Phys.*, **57**, 72–91.

Gerber, H. E., 1981: Microstructure of a radiation fog. *J. Atmos. Sci.*, **38**, 454–458.

Gurka, J. J., 1978: The role of inward mixing in the dissipation of fog and stratus. *Mon. Wea. Rev.*, **106**, 1633–1635.

Gustafson, A. V., and S. T. Wasserman, 1976: Use of satellite infor-

mation in observing and forecasting fog dissipation and cloud formation. *Mon. Wea. Rev.*, **104**, 323–324.

Holets, S., and R. N. Swanson, 1981: High-inversion fog episodes in central California. *J. Appl. Meteor.*, **20**, 890–899.

Kamiko, T., and M. Okano, 1971: Cellular cloud pattern. *Geophys. Mag.*, **35**, 275–292.

Kelley, R. D., 1983: Time-evolution of horizontal roll geometries over Lake Michigan. *Conf. Cloud Physics*, Chicago, IL, Amer. Meteor. Soc., 20–23.

Krishnamurti, R., 1975: On cellular cloud patterns. Part 3: Applicability of the mathematical and laboratory models. *J. Atmos. Sci.*, **32**, 1373–1383.

Kuettner, J. P., 1971: Cloud bands in the earth's atmosphere. *Tellus*, **23**, 404–425.

Lala, G. G., J. E. Jiusto, M. B. Meyer and M. Kornfield, 1982: Mechanisms of radiation fog formation on four consecutive nights. *Proc. Conf. Cloud Physics*, Amer. Meteor. Soc., Chicago, IL, 9–11.

LeMone, M. A., 1976: Modulation of turbulence energy by longitudinal rolls in an unstable planetary boundary layer. *J. Atmos. Sci.*, **33**, 1308–1320.

Pellew, S., and R. V. Southwell, 1940: On maintained convective motion in a fluid heated from below. *Proc. Roy. Soc. London.*, **A176**, 966.

Pilie. R. J., E. J. Mack, W. C. Kocmond, W. J. Eadie and C. W. Rogers, 1975: The life cycle of a valley fog: II. Fog microphysics. *J. Appl. Meteor.*, **14**, 364–374.

Plank, V., 1969: The size distribution of cumulus clouds in representative Florida populations. *J. Appl. Meteor.*, **8**, 46–67.

Roach, W. T., 1976: On the effect of radiative exchange on the growth by condensation of a cloud or fog droplet. *Quart. J. Roy. Meteor. Soc.*, **102**, 361–372.

——, R. Brown, S. J. Caughey, J. A. Garland and C. J. Readings. 1976: The physics of radiation fog. Part I: A field study. *Quart. J. Roy. Meteor. Soc.*, **102**, 313–333.

Robinove, C. J., 1982: Computation with physical values from Landsat digital data. *Phot. Eng. Rem. Sens.*, **48**, 781–784.

Taylor, G. F., 1941: *Aeronautical Meteorology.* Putman, 455 pp.

Vinnichenko, N. K., N. Z. Pinus, S. M. Shmeter and G. N. Shur, 1973: *Turbulence in the Free Atmosphere.* Consultants Bureau, NY. 263 pp.

Walter, B. A., Jr., and J. E. Overland, 1984: Observations of longitudinal rolls in a near neutral atmosphere. *Mon. Wea. Rev.*, **112**, 200–208.

Welch, R. M., and M. G. Ravichandran, 1985: Prediction of quasi-periodic oscillations in mature radiation fogs. *J. Atmos. Sci.*, **42**, 2888–2897.

Wielicki, B. A., and R. M. Welch, 1985: Cumulus cloud properties derived using Landsat satellite data. *J. Climate Appl. Meteor.*, **25**(3, in press).

END

DTIC

8-86